Journal of Molecular Structure 1232 (2021) 130074

Contents lists available at ScienceDirect

Journal of Molecular Structure

journal homepage: www.elsevier.com/locate/molstr

Effective inhibition of mild steel corrosion by 6-bromo-(2,4-dimethoxyphenyl)methylidene]imidazo [1,2-a]pyridine-2-carbohydrazide in 0.5 M HCl: Insights from experimental and computational study

K Vranda Shenoy[a], Pushyaraga P Venugopal[b], P D Reena Kumari[a,*], Debashree Chakraborty[b,**]

[a] Department of Chemistry, Shri MadhwaVadiraja Institute of Technology and Management, Bantakal, Udupi, Karnataka, India
[b] Biophysical and Computational Chemistry Laboratory, Department of Chemistry, National Institute of Technology Karnataka, India

ARTICLE INFO

Article history:
Received 6 November 2020
Revised 1 February 2021
Accepted 3 February 2021
Available online 6 February 2021

Keywords:
Corrosion inhibitor
Mild steel
Electrochemical study
Langmuir's adsorption isotherm
DFT studies

ABSTRACT

A new inhibitor, 6-bromo-(2,4-dimethoxyphenyl)methylidene]imidazo [1,2-*a*]pyridine-2-carbohydrazide (DMPIP) was evaluated as a corrosion inhibitor for Mild Steel (MS) in 0.5 M HCl solution at 303–323 K using potentiodynamic polarization and electrochemical impedance spectroscopic (EIS) techniques. Both the techniques confirmed an increase in inhibition efficiency with the concentration of DMPIP but decrease with temperature. The highest inhibitive action (96.7%) was registered at 303 K for 500 ppm of DMPIP concentration. Polarization study revealed mixed inhibition action by DMPIP. Nyquist plot obtained for MS using EIS technique showed two capacitive loops on addition of inhibitor to HCl solution confirmed the inhibitory action of DMPIP via adsorption at the metal/solution interface. The surface morphology analysis was carried out by SEM, EDX and FTIR techniques. The adsorption process was demonstrated using Langmuir's adsorption isotherm model. The thermodynamic parameters (ΔG^{o}_{ads}, ΔH^{o}_{ads}) indicated that the adsorption was spontaneous and done by physisorption. Further, quantum chemical studies using Density Functional Theory (DFT) elucidated that the formation of Fe-DMPIP complex presumably due to the interaction of protonated form of DMPIP with the empty *d* orbitals of the iron atom.

1. Introduction

Mild steel (MS) consists of less than 0.3% of carbon content, which is the most commonly used forms of steel in many industrial applications as a construction component in building industry, automobile industry, petroleum industry, power plants, etc. due to its advantageous features like malleability, ductility, high strength as well as low cost. But dissolution process is high in presence of acidic media during industrial processing like cleaning, pickling due to low resistance of mild steel for an acid attack. Among the various measures applied to protect metals from the aggressiveness of acid, the use of inhibitors is considered as one of the most practical, easily operative and cheapest methods [1,2]. By definition, corrosion inhibitors are substances which are soluble in an aggressive solution, without participating in the overall reaction reduces the corrosion rate of the metal. From literatures, it is found that various organic compounds have been utilized as corrosion inhibitors for MS in HCl solution, such as organic dyes [3], ionic liquids [4], nonionic surfactants [5], gemini surfactants [6,7], natural polymers [8,9], carbaxmide ligands [10], natural compounds [11,12], polysaccharides [13,14],extracts of natural substances [15–18], polypeptides [19]amino acids [20,21], Schiff bases [22,23]. The inhibitor efficiency depends on the nature of corrosion medium, the nature of metal surface, electrochemical potential at the interface, and also on the geometrical configuration of the inhibitor [24,25].

Heterocyclic compounds are considered as an efficient organic corrosion inhibitor against metal in an aggressive medium [26]. Due to the presence of aromatic rings, electron-donating groups, polar molecules, and pi bonds along with the electronegative heteroatoms such as nitrogen, oxygen, sulfur. They may act as barrier by forming an adsorbed layer on the metal surface or retard the

* Corresponding author at: Chemistry laboratory, Department of chemistry, Shri MadhwaVadiraja Institute of Technology and Management, Bantakal, Udupi affiliated to VTU, Balagavi, Karnataka 574 115, India.
** Corresponding author at: Biophysical and Computational Chemistry Laboratory, Department of Chemistry, National Institute of Technology Karnataka, Surathkal, Mangalore 575025, India.
E-mail addresses: reena.chemistry@sode-edu.in (P.D. Reena Kumari), debashree@nitk.edu.in (D. Chakraborty).

https://doi.org/10.1016/j.molstruc.2021.130074
0022-2860/

cathodic, anodic or both the reaction.Thus blocking the active corrosion centers and decreases the corrosion rate [27,28].

Imidazo [1,2-a] pyridines are the important class of heterocyclic compounds, find great importance in the pharmaceutical industry as a bioactive molecule like antiviral [29], antifungal [30], antibacterial [31], anti-inflammatory, analgesic and antipyretic [32]. Schiff bases of imidazo pyridines are also important compounds due to its biological activity such as antibacterial [33], antimalarial [34,35], antifungal [36], and anticonvolusant [37]. But recently imidazo pyridine derivatives and Schiff bases of imidazo pyridines are also reported as corrosion inhibitors for mild steel in HCl medium with different substituent position and group due to its ability to donate electrons as well as a possible back donation which affects the corrosion rate and increases inhibition efficiency [23,38–42].

A review of the literature reveals that the structural modifications by incorporating different functionalities in their structure largely improve their applicability as potential corrosion inhibitors [43,44]. Therefore the objective of the present work is to inspect the utilization of the newly synthesized imidazo [1,2-a] pyridine derivative *viz* 6-bromo-(2,4-dimethoxyphenyl)methylidene]imidazo [1,2-*a*]pyridine-2-carbohydrazide (DMPIP) as corrosion inhibitor for MS in 0.5 M HCl solution. Commonly, Hydrochloric acid is preferred as pickle liquor during the surface cleaning of iron alloys or steel surfaces due to its desired surface cleaning effect. However, at higher concentrations of HCl, hydrogen embrittlement becomes a problem for mild steel and that leads to considerable degradation of mechanical properties [45]. Hence, acid concentration and solution temperature must be kept under control to ensure the desired pickling rates.

Thus the inhibitory behavior of 6-bromo-(2,4-dimethoxyphenyl)methylidene]imidazo [1,2-*a*]pyridine-2-carbohydrazide (DMPIP) was systematically evaluated for MS in 0.5 M HCl solution at 303–323 K using potentiodynamic polarization curves, electrochemical impedance spectroscopy (EIS), scanning electron microscopy (SEM), Energy-dispersive X-ray spectroscopy (EDX), Fourier Transform Infrared Spectroscopy (FT-IR), and quantum chemical calculations. To get an insight on the adsorption mechanism of the inhibitor on metal surface temperature effect, kinetic, and thermodynamic parameters (E_a, K_{ads}, ΔG°_{ads}) were considered. The correlation between molecular structure and inhibition properties were investigated using quantum chemical parameters. Also, various quantum indices related to the molecule were studied and compared with the experimental inhibitive efficiency data of DMPIP.

2. Experimental

2.1. Materials and methods

The MS coupons with following composition (wt.%): C 0.18%, Mn 0.6%, S 0.05%, P 0.04%, Si 0.1%, and remaining of iron were used for electrochemical study. The epoxy resin embedded mild steel strip of 0.502 cm^2 of area was exposed to the medium for investigation. Before the experiment, test coupon was abraded with 500 to 2000 grade silicon carbide papers successively, then washed and rinsed with doubly distilled water, immersed in acetone followed by air drying. The electrolyte solution, 0.5 M HCl, was prepared using analytical grade 37 wt% HCl (Merck) and suitable volume of purified water. The concentration of DMPIP used for this investigation ranged from 50–500 ppm (mg/L) by weight in 100 mL of the test solution. The testing solution was kept under aerated condition at 303–323 K successively by using a water thermostat.The molecular structure of DMPIP is shown in Fig. 1(a). The molecule was synthesized using the reported procedure [37]; the reaction scheme for the synthesis is shown in Fig. 1(b). The molecule was characterized by melting point (Digital melting point apparatus EQ 730 by Equiptronics) and FT-IR spectra as shown in Fig. 1(c) (Bruker Instruments, frequency range 500 cm^{-1} to 4000 cm^{-1})

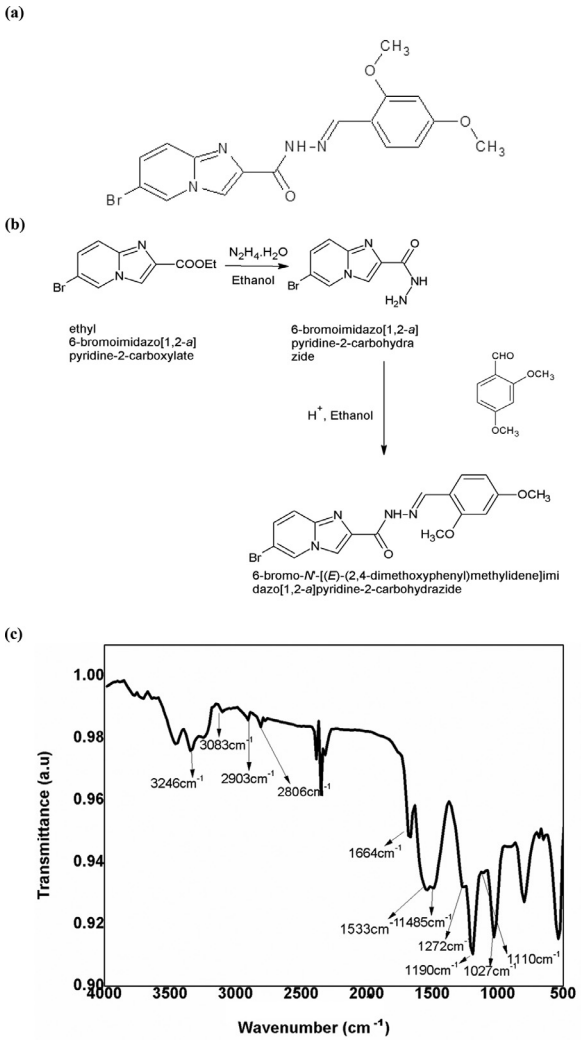

Fig. 1. (a) Structure of 6-bromo-(2,4-dimethoxyphenyl)methylidene]imidazo[1,2-*a*]pyridine-2-carbohydrazide **(b)** Reaction Scheme for the synthesis of 6-bromo-(2,4-dimethoxyphenyl)methylidene]imidazo[1,2-*a*]pyridine-2-carbohydrazide **(c)** FT-IR spectrum for DMPIP inhibitor in the frequency range 500 cm^{-1} to 4000 cm^{-1}.

Melting Point: 252–258 °C. FTIR **(ATR, cm^{-1}):** 3246 (N–H), 3083 (Ar-C), 2903 ($O–CH_3$), 2806 ($O–CH_3$), 1664 (C=O), 1533 (C=N), 1485 (C=C), 1272 (C–O-C), 1190 (C–N), 1110 (C–O-C) and 1027 (C-Br) (Fig. 1(c)).

Electrochemical studies were carried out in a conventional three-electrode cell consisting of a saturated calomel electrode (SCE) as the reference electrode, platinum electrode as an auxiliary electrode (CE), and cylindrical MS coupons coated with epoxy resin as a working electrode (WE), using CH electrochemical workstation (Model No: CHI 608E) manufactured by CH Instruments, Austin, USA. The finely polished test coupons were dipped in 0.5 M HCl possessing 50 ppm, 100 ppm, 200 ppm and 500 ppm of DMPIP at the temperature range of 303–323 K. Before each experiment, the working electrode was immersed in the test solution for 1800 seconds to reach the quasi-equilibrium state. The relationships between open circuit potential (OCP) values and immersion time for MS in 0.5 M HCl solution without and with DMPIP at 303 K are shown in Fig. 2. It is clear that the OCP values remains almost constant after 1000 s indicating the system under study has reached the steady state. Thus all the electrochemical tests were performed after 30 min immersion in the corresponding test solution.

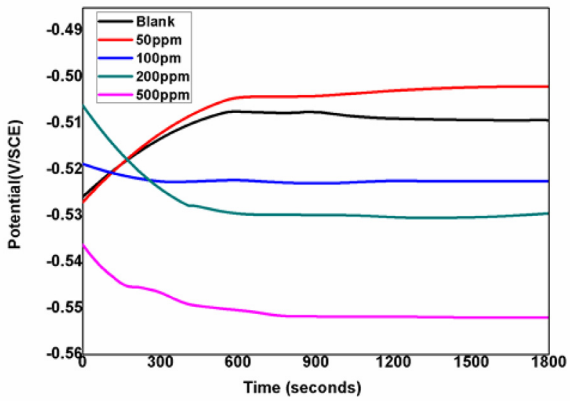

Fig. 2. Open Circuit Potential values versus Time for MS in 0.5 M HCl with and without inhibitor.

Polarization curves were obtained in the potential range from −200 to +200 mV after establishing the OCP with a scan rate of 1 mVs^{-1}. All the reported potential values were referred to SCE. The corrosion current density (i_{corr}) values were obtained by the Tafel extrapolation method. The electrochemical impedance measurements were performed in the frequency range of 100 kHz to 10 mHz with 5 mV amplitude at OCP. EIS data were investigated and then analyzed using Zsimpwin software. Reproducibility checked at least three times for each experimental setup, and the average values were taken and presented.

2.2. Quantum chemical study

Density functional theory (DFT) calculations are considered as the "green corrosion inhibition method" which helps to understand the molecular structure and its corrosion inhibition behavior. The electronic/molecular properties and reactivity indices of the inhibitor can accurately predict its corrosion inhibition efficiency. Correlation between experimental investigations regarding inhibition efficiency and theoretical calculations helps in understanding the observed experimental behavior of the inhibitor by studying the molecular structure. DFT was used to analyze the electronic properties of the DMPIP molecule in its neutral and protonated forms in aqueous phase by Becke's three-parameter exchange functional theory with the Lee–Yang–Parr non local correlation functional (B3LYP) [46] and 6–311++G(d, p) [47] basis set in Gaussian09 program package using SCF approach. Quantum chemical parameters associated with energies such as energy of highest occupied molecular orbital (E_{HOMO}), energy of lowest unoccupied molecular orbital (E_{LUMO}) and energy gap (ΔE_{gap}) have been assessed. Other chemical parameters like electronegativity (χ), electron affinity (A), ionization energy (I), global softness (σ), global hardness (η), dipole moment (μ) and the fraction of electrons transferred (ΔN) were also studied. Mulliken charge distribution and Fukui indices were calculated to analyze the local reactive sites on the inhibitor molecule.

2.3. Surface morphology investigations

SEM images and EDX images of the test samples were recorded and analyzed after exposure to 0.5 M HCl solution in the absence and presence of DMPIP for 15 h using SEM model Carl Ziess FE-SEM and Oxford instruments respectively. The adsorption of DMPIP on MS was elucidated by probing the surface of the working electrodes using FTIR spectroscopic technique. Bruker instruments spectrometer in the frequency range of 500 cm^{-1} to 4000 cm^{-1} used for FTIR analysis to study the FTIR data related to DMPIP inhibitor and that of obtained from the surface of the MS copouns immersed in 0.5 M HCl solution containing 500 ppm DMPIP for 15 h at 298 K were recorded.

3. Results and discussion

3.1. Tafel polarization study

The electrochemical kinetics of corrosion process was studied using Tafel polarization study in absence and presence of varying concentrations (50–500 ppm) of DMPIP in 0.5 M HCl solution. The corrosion potential (E_{corr}) and corrosion current density (i_{corr}), slope of the cathodic branch (β_c) and slope of the anodic branch (β_a) were acquired from tafel polarization curves. The rate of corrosion (ν_{corr}) was calculated from i_{corr} using expression 1 [48,49].

$$\nu_{corr}\ \left(mm\ y^{-1}\right) = \frac{3270\ \times M \times i_{corr}}{q \times Z} \tag{1}$$

where 3270 is a constant of corrosion rate, i_{corr} refers corrosion current density (A cm^{-2}), q is the corroding material density (g cm^{-3}), M is the metal atomic mass and Z is the number of electrons transferred/atom. Eq. (2) is used to calculate the percentage of inhibition efficiency (η%).

$$\eta\% = \frac{i^{0}_{corr} - i_{corr}}{i^{o}_{corr}} \times 100 \tag{2}$$

where, i°_{corr} and i_{corr} are values of corrosion current density values for blank solution and solutions with various concentrations of DMPIP, respectively. From Fig. 3(a), it is visible that the nature of polarization curves remains unchanged both in uninhibited and inhibited solution. But in the presence of DMPIP and as the concentration was increased, the polarization branches shifted toward lower current density region indicating slowdown of the electrochemical reactions. The related experimental parameters are listed in Table 1, shows that as the concentration of the inhibitor increases, i_{corr} decreases, correspondingly, η% increases. However, an increase in the ν_{corr} with temperature suggests decreased inhibition efficacy by DMPIP molecules on MS surface at higher temperatures. DMPIP recorded best inhibition efficiency (96.79%) at 500 ppm at 303 K, indicating that at this optimum concentration, DMPIP can provide more significant inhibitor protective effect against metal corrosion. Higher temperature tafel plots for 313 K and 323 K are given in Supplementary Information (Figure S1 and Figure S2).

Table 1, reveals that there was no noticeable shift in corrosion potential values ($E_{corrinh}$) were observed after the addition of DMPIP with concerning to the corrosion potential values ($E_{corrblank}$) of blank solution. Normally, inhibitors can be arranged as either anodic or cathodic if the shifting of $E_{corrinh}$ values exceeds ± 85 mV compared to the $E_{corrblank}$ values [50]. However, in this work, maximum displacement was less than ± 85 mV; hence, DMPIP can be classified as mixed-type inhibitor controlling both dissolutions of metal and hydrogen liberation reactions [51,52]. Additionally, to get more insight of the inhibition mechanism all the polarization plots were displaced to the zero potential ($E_{corr} = 0$) as shown in Fig. 3(b). The displacement of both of the cathodic and anodic current densities towards lower current densities at different concentrations of DMPIP evidence a mixed inhibition effect on the MS [18,53]. At higher concentrations of inhibitor, the i_{corr} values decrease more predominantly suggesting the more or less complete isolation of metal surface from the aggressive media by forming a protective barrier due to the accumulation of a higher number of DMPIP molecules at the MS surface which provides wider surface coverage area.

As it can be noted from Table 1, compared with the blank solution, the anodic Tafel slopes (β_a) for inhibitors exhibit the ob-

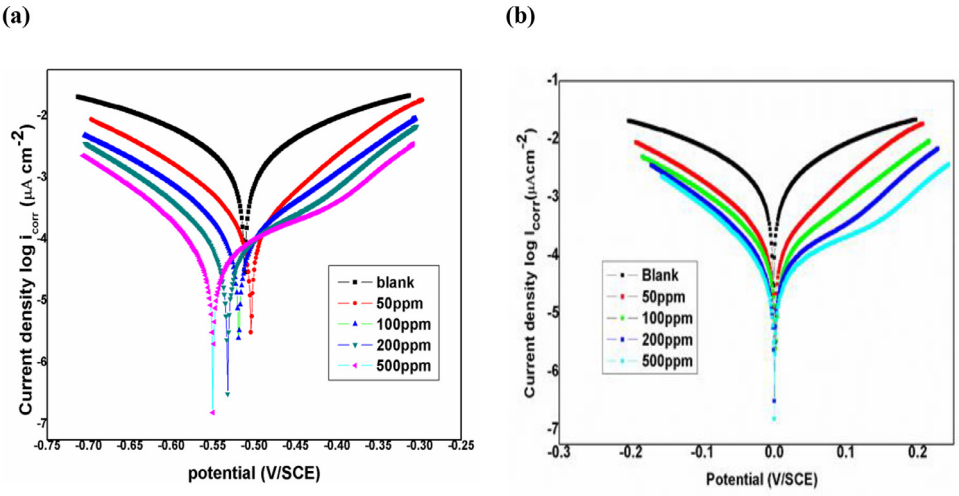

Fig. 3. Tafel curves for MS corrosion without and with DMPIP inhibitor in 0.5 M HCl solution at 303 K (a) Original E_{corr}, (b) Displacement of E_{corr} to the zero potential.

Table 1
Potentiodynamic polarization parameters for the MS corrosion in 0.5 M HCl without and with DMPIP at 303–323 K.

Temperature (K)	Inhibitor conc (ppm)	β_a (mV)	β_c (mV)	E_{corr} (mV)	i_{corr} (μA cm^{-2})	v_{corr}(mm y^{-1})	(η%)
303	**Blank**	175	174	−510	2805	32.56	
	50	131.5	150	−502	830	9.65	70.35
	100	121.6	138	−524	401	4.01	86.78
	200	117	117	−532	151	1.51	95.01
	500	152	111	−551	96.7	0.97	96.79
313	**Blank**	182	186	−501	3400	39.54	
	50	138	148	−495	1100	12.79	67.64
	100	135	144	−512	620	7.21	81.76
	200	149	138	−519	265	3.08	92.20
	500	162	134	−544	165	1.91	95.14
323	**Blank**	194	197	−504	3800	44.19	
	50	175	181	−511	1350	15.70	64.47
	100	147	153	−518	1010	11.74	73.42
	200	160	143	−526	594	6.90	84.36
	500	188	151	−537	410	4.76	89.21

vious decrease noticeably at lower concentrations of DMPIP (50–100 ppm), which is more remarkable at $T = 303$ K. This suggests for low concentrations, the adsorption is preferentially at the anodic sites leading tothe formation of Fe–Inh complex compound which influences the dissolution of Fe. On the other hand, further enhancement of η% with increasing inhibitor concentration (200–500 ppm) suggests that DMPIP molecules impede iron dissolution likely by blocking off the anodic reactive sites [54]. But, insignificant decrement of cathodic Tafel slopes (β_c) concerning the blank indicating that the hydrogen evolution process is activation controlled, and the addition of DMPIP reduce the kinetics of cathodic reaction by blocking the active cathodic sites without changing the mechanism of this process [11,13].This is further supported by the parallel cathodic plots of the inhibited solution to the cathodic branch of the blank solution (Fig. 3(a)) while the shape and slope of the anodic plots were changed significantly with the addition of DMPIP, revealing the impact of the additives on the iron dissolution mechanism. [18].

3.1.1. Thermodynamic and activation parameters

The data in Table 1 shows a linear association of corrosion rate with temperature. The influence of temperature on corrosion rate without and with inhibitors is expressed by Arrhenius Eq. (3). The graphical representation of ln v_{corr} vs. $1/T$ at different concentrations of DMPIP is given in Fig. 4. [55].

$$lnv_{corr} = \frac{-E_a}{RT} + lnA \quad (3)$$

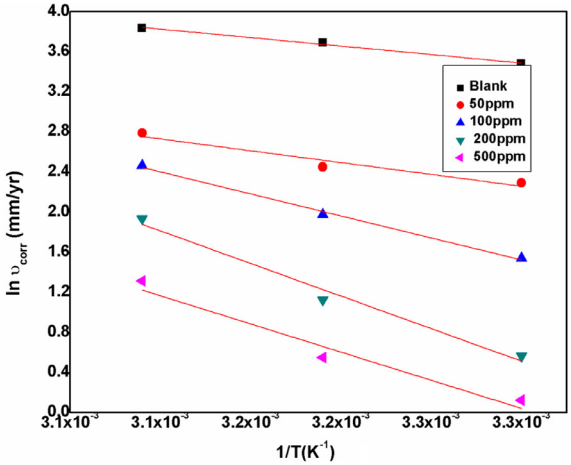

Fig. 4. lnv_{corr}*vs* $1/T$ for MS corrosion in 0.5 M HCl solution with various concentrations of DMPIP.

where $E_a$is the energy of activation for MS dissolution in 0.5 M hydrochloric acid solution, R terms for universal gas constant, T refers to absolute temperature (K), and A denotes the frequency factor.

The slope of the straight line obtained in Fig. 4 was used to calculate the E_a value for the dissolution of MS in acid solution. The data in Table 2 indicates that the E_a values in the solution with

Table 2
Activation energy parameters of DMPIP in 0.5 M HCl.

Inh. Conc (ppm)	E_a(kJ mol^{-1})	ΔH^*(kJ mol^{-1})	ΔS^*(J mol^{-1} K^{-1})
Blank	14.675	11.35	−178.54
50	19.621	17.27	−168.86
100	36.506	33.98	−120.22
200	54.024	51.49	−70.81
500	47.572	44.23	−98.70

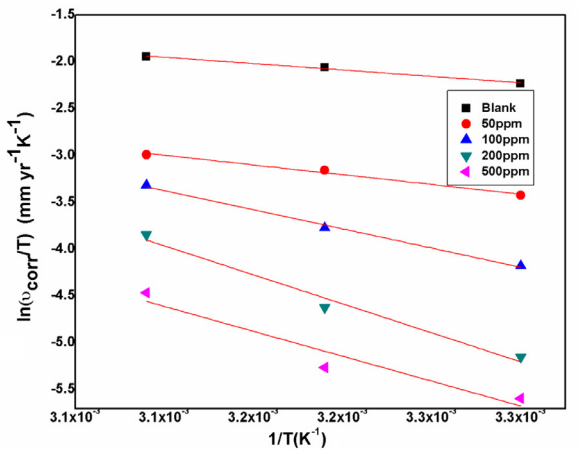

Fig. 5. Plot of ln v_{corr}/T versus $1/T$ for MS in 0.5 M HCl solution with different concentrations of DMPIP.

different concentrations of DMPIP exceed than that of the blank solution. This suggests that the presence of DMPIP influences the energy barrier for the corrosion process of MS by reducing corrosion rate and consequently increasing the $\eta\%$. A higher value of E_a for inhibited solution with reference to blank suggests physical adsorption of DMPIP at the MS surface. In addition, a low value of E_a (47.57 kJ mol^{-1}) at the optimum concentration (500 ppm) of the inhibitor suggests stability of corrosion product formed at the metal/solution interface [56]. Further, higher values of E_a (19.62 to 47.57 kJ mol^{-1}) in the presence of inhibitor could be attributed for a considerable decrease in adsorption and increase in desorption/dissolution of the DMPIP molecules with the rise in temperature leading to increase the corrosion rate owing to the direct contact of the bare metal surface with acid [57].

The values of enthalpy of activation (ΔH^*) and entropy of activation (ΔS^*) for metal dissolution were obtained from Eq. (4). [55].

$$v_{corr} = \frac{RT}{Nh} exp\left(\frac{\Delta S^*}{R}\right) exp\left(-\frac{\Delta H^*}{RT}\right) \quad (4)$$

Where, h refers to Planck's constant, and N gives the number of Avogadro. The plots of $\ln v_{corr}/T$ versus $1/T$ gave straight line as shown in Fig. 5. ΔH^* and ΔS^* were calculated from the slope $(-\Delta H^*/R)$ and intercepts $(\ln R/Nh + \Delta S^*/R)$ respectively are listed in Table 2. The positive values of ΔH^* reflects the endothermic nature of dissolution of MS in the presence of DMPIP [58,59] whereas higher values in solution with varied inhibitor concentrations compared to blank solution advocate its inhibitive actions to check the electrochemical dissolution of MS in acid solution. The values of ΔS^* for the solutions in presence of DMPIP are more positive than that of the blank solution indicates an increase in the randomness of the dissolution process of metal in the presence of acid, which is the driving force for the adsorption of inhibitor on MS surface to form the activated complex [60–62]. For uninhibited solution, the rate-determining step of the transition state represents the orderly arrangement than in the initial state. The adsorption of the

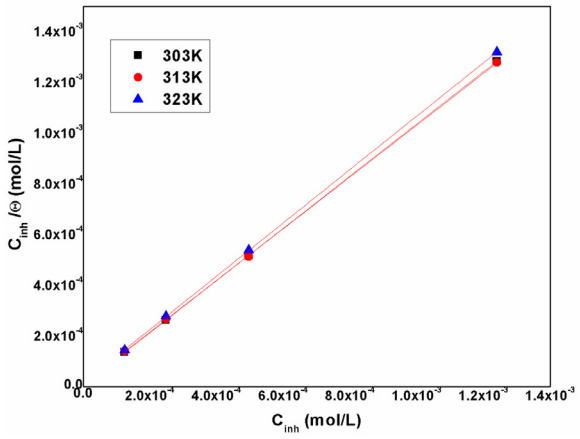

Fig. 6. Langmuir adsorption isotherm model of DMPIP on the MS in 0.5 M HCl at 303–323 K.

inhibitor DMPIP molecules on the MS surface from the hydrochloric acid solution retards the hydrogen ion discharge from the metal surface, which is the rate-determining step.

3.1.2. Adsorption isotherm

Two types of adsorption modes are generally possible during the corrosion inhibition process. Physical adsorption or physisorption and chemisorption. In physisorption, there are weak electrostatic interactions between the organic ions or dipoles of the inhibitor and charged metal surface while in chemisorption, the electron sharing or transfer occurs between inhibitor and metal surface to form a strong coordinate bond.

Corrosion inhibition involves interactions at the metal/electrolyte interface which is totally a surface phenomenon. The degree of surface coverage θ for various concentrations of the additives was obtained from Eq. (5) and it was employed to fit graphically for different adsorption isotherms such as Freundlich, Frumkin, Temkin, Flory-Huggins, Langmuir, etc.

$$\theta = \frac{\eta\%}{100} \quad (5)$$

From all the tested models, the best correlation between experimental data and isotherm function was obtained for the Langmuir isotherm with the slopes and linear regression coefficients (R^2) close to unity. The plot of C_{inh}/θ versus C_{inh} is represented in Fig. 6. Langmuir isotherm model is expressed using Eq. (6) [63–65].

$$\frac{C_{inh}}{\theta} = \frac{1}{K_{ads}} + C_{inh} \quad (6)$$

where C_{inh} is the concentration of inhibitor, K_{ads} is the adsorption-desorption process equilibrium constant.

The K_{ads} equilibrium constant, obtained from the intercepts of the straight lines in the Fig. 6, represents the strength of interaction between adsorbed inhibitor and surface of the MS. Larger values of K_{ads} shows higher effectiveness of adsorption and better protection efficiency obtained by the inhibitor. In the present study, K_{ads} value is more at room temperature (Table 3) showing efficient corrosion inhibitive action by the inhibitor. K_{ads} is related to the standard free energy change during the adsorption process, ΔG°_{ads}, and using Eq. (7) [66]:

$$\Delta G^o_{ads} = -RT ln(K_{ads} \times 55.5) \quad (7)$$

Where, R is the universal gas constant (8.314 J^{-1} mol^{-1} K) and T is the absolute temperature and 55.55 is the molar concentration of water in solution (mol L^{-1}). The standard enthalpy

Table 3
Adsorption parameters for MS for DMPIP inhibitor in 0.5 M HCl solution.

Temperature (K)	$K_{ads\ (10^4)\ M}$	Slope	ΔG°_{ads}(kJ mol^{-1})	ΔH°_{ads}(kJ mol^{-1})	ΔS°_{ads}(J mol^{-1} K^{-1})
303	118.9	1.02	−39.5		
313	81.23	1.00	−39.9	−27.7	−40.0
323	61.44	1.07	−40.3		

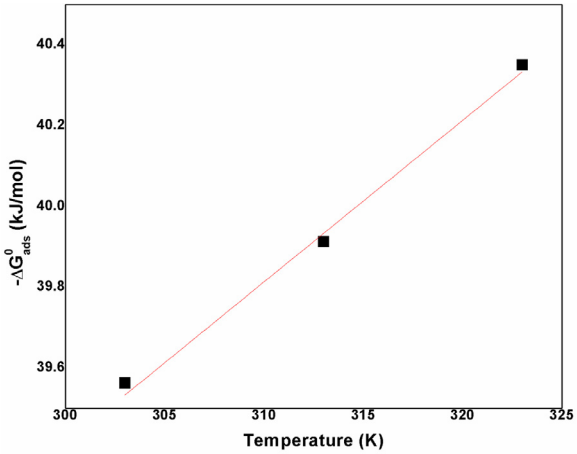

Fig. 7. Relationship between ΔG°_{ads} and T.

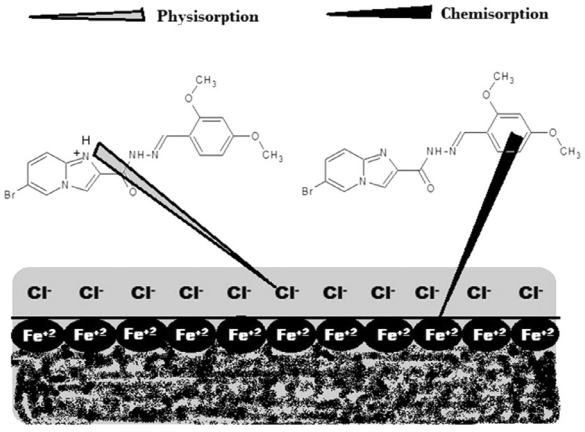

Fig. 8. Interaction of metal with inhibitor showing physisorption and chemisorption process.

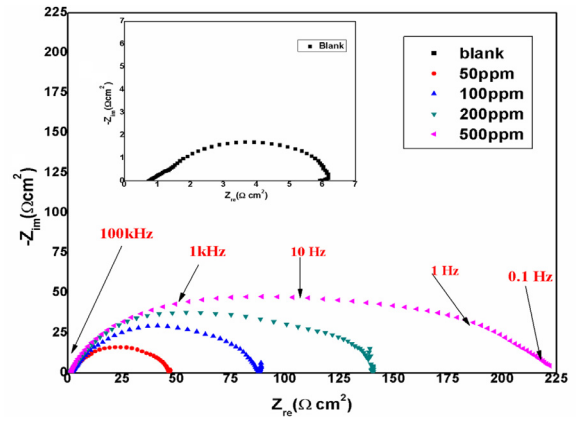

Fig. 9. Nyquist plot for MS in 0.5 M HCl solution without DMPIP and with different concentration of DMPIP at 303 K.

change (ΔH°ads), standard entropy change (ΔS°ads) of adsorption of DMPIP on MS surface is calculated using Eq. (8) [67]:

$$\Delta G^{0}_{ads} = \Delta H^{0}_{ads} - T\Delta S^{0}_{ads} \quad (8)$$

The plot of ΔG^{0}_{ads} vs T gives a straight line (Fig. 7), with slope equal to $-\Delta S^{0}_{ads}$ and intercept ΔH^{0}_{ads}.

The thermodynamic parameters are listed in Table 3 for the adsorption of DMPIP on MS surface. ΔG°_{ads} values are negative ensured adsorption of DMPIP molecules on the electrode surface is spontaneous and strength of interactions is high between the charged inhibitor and metal surface. Generally, if the values of ΔG°_{ads} are around −20 kJ mol^{-1} or more positive, it is said to be physical adsorption process and if it is around −40 kJ mol^{-1} or more negative, then it is termed as chemisorption [68,69]. However, the value of −40 kJ mol^{-1} is referred to as threshold value between physisorption and chemisorption [70].

The calculated ΔG°_{ads} values (Table 3) are in the range of −39.5 to −40.3 kJ mol^{-1} for the studied range of temperatures which indicates that the adsorption involves both physisorption as well as chemisorption process. Indeed, the corrosion inhibition by the DMPIP molecule on mild steel attributed as physisorption process since activation energy values are high for inhibited solution compared to the blank. Initially, adsorption might occur by physisorption due to adsorbed water molecule on the MS surface, which is followed by chemical interaction with the inhibitor molecules by replacing the water molecules on the metal surface [71]. In hydrochloric acid medium, Cl^{-} ions also compete for the adsorption along with the organic inhibitors and itis thought that absorbable anions like chloride ions are adsorbed on the electrode surface through creating oriented dipoles [72]. Thus, the negatively charged MS surface attracts the cationic inhibitor species resulting in the electrostatic accumulation of protonated DMPIP molecules onto the Cl^{-} adsorbed steel surface. While in chemisorption type, the protonated inhibitor donates electrons to the metal by losing proton as shown in Fig. 8 [10].

An exothermic adsorption process is confirmed by the negative ΔH°_{ads}values (Table 3). According to the earlier reported works, if the value of ΔH°_{ads} is less than or equal to −40 kJ mol^{-1} refers to physisorption and more than −100 kJ mol^{-1} for chemisorption process [73,74]. Therefore, though the above theory (based on ΔG°_{ads} values) suggests both physical and chemical adsorption of DMPIP molecules on the MS surface the lower threshold value of ΔH°_{ads} (−27.7 kJ mol^{-1}) confirms that DMPIP molecules are mainly adsorbed on the MS surface through physisorption phenomenon. The entropy of adsorption, ΔS°_{ads} calculated is found to be negative, suggesting decrease in the disorderness from the reactant to the adsorbed species. The adsorption nature of the inhibitor and the guiding energy were further evaluated from short vaccum MD simulations and the detailed results are given in Supplementary Information (Figure S3 and Figure S4).

3.2. Electrochemical Impedance spectroscopy (EIS)

In order to study the kinetics and characters of electrochemical reactions for mild steel, the EIS analysis was done. Fig. 9 represents the Nyquist plot obtained at OCP, while Table 4 summarizes the impedance data for MS in the absence and presence of different concentrations of inhibitor DMPIP at 303 K in 0.5 M HCl solution. Nyquist plots show depressed capacitive loops with center under the real axis resulted due to roughness and inhomogeneities

Table 4
EIS parameters for the corrosion of MS in 0.5 M hydrochloric acid medium having different concentrations of DMPIP at 303–323 K.

Temperature (K)	Inhibitor Concentration (ppm)	R_s (Ωcm^2)	R_f (Ωcm^2)	R_{ct} (Ωcm^2)	CPE_{dl} (10^{-4}) ($\mu F cm^{-2}$)	χ^2 (10^{-3})	η%
303	**Blank**	0.83		10.8	5.36	4.7	
	50	0.67	3.7	33.1	2.42	0.69	67.37
	100	0.6	5.3	74.98	2.70	2.1	85.59
	200	0.7	4.4	138	1.49	3.2	92.17
	500	0.6	4.3	210	1.46	4.1	94.85
313	**Blank**	0.74		8.7	8.99	2.0	
	50	0.5	3.8	21.95	5.62	0.24	60.36
	100	0.65	5.9	53.55	5.35	1.5	83.75
	200	0.8	14.6	121	4.58	1.01	92.80
	500	0.6	28.1	127	2.04	1.3	93.14
323	**Blank**	0.73		7.01	9.62	2.0	
	50	1.2	6.8	15.61	6.29	0.97	55.09
	100	0.33	4.6	29.22	5.82	1.7	76.00
	200	0.22	8.6	41.35	5.22	2.1	83.04
	500	0.7	14.08	59.8	1.78	0.46	88.27

on the solid surface [75,76]. As compared to the blank solution, the diameter of the semi-circles in the Nyquist plot increases for inhibited solutions with increasing concentration of the inhibitor. These results confirm the inhibitory action of DMPIP molecules at the MS surface.

Fig. 10 represents the equivalent circuit for the mild steel dissolution process to analyze the electrochemical data using Zsimpwin 3.2.1 software. It is observed that an acceptable accuracy of the fitting was obtained, as evidence by Chi-square (χ^2) in the order of 10^{-3} for all the experimental data as shown in Table 4. On addition of DMPIP inhibitor, impedance response changes significantly in hydrochloric acid media showing two capacitive loops in its Nyquist plot. The response of the EIS spectrum presented here shows similarity with the previous reports [13,16,54,77,78]. Wang et al. [78] explained that one capacitive loop formed due to the double layer capacitance at higher frequency ranges and the other is due to the continuous adsorption and desorption process at lower frequencies. Due to the non-ideal capacitive behavior, which is commonly encountered during the electrochemical studies of solid/liquid interfaces, it is necessary to replace an ideal capacity (C_{dl}) by a constant phase element CPE_{dl} while fitting the EIS data as shown in Fig.10(b) and (d) [79]. The fitting result (Table 4) shows that R_{ct} (charge transfer resistance) and R_f (protective film resistance) increases with increasing DMPIP concentration and CPE_{dl} (double layer capacitance) values decrease at higher frequencies inferring that adsorption of inhibitor molecule on the MS surface of the electrode increases [80]. *CPE* is mathematically expressed as following equation [54]:

$$Z_{CPE} = Y_o^{-1}(j\omega)^{-n} \quad (9)$$

Where Y_o is the magnitude of the *CPE*, j is the imaginary unit, ω is the angular frequency, and n is the phase shift gives details about the degree of surface inhomogeneity [54,79].

The CPE_{dl} values decreased with the addition of DMPIP as it is evident from Table 4 ascribed due to the reduction in local dielectric constant or increase in the thickness of the protective layer at the solid/solution interface region. In other words the gradual replacement of the adsorbed water molecules at the steel surface by DMPIP molecules with lower dielectric constant leading to lower value of CPE_{dl} [81]. It is apparent from Fig. 9 that the radius of the capacitive loop is increased with the increase of DMPIP concentration suggesting enhanced impediment of the surface film for charge transfer process at the metal-solution interface. R_{ct} and R_f values are found to increase with additives concentration presumably due to the increased imperviousness of the protective film on the steel surface. The η% was calculated from the charge transfer

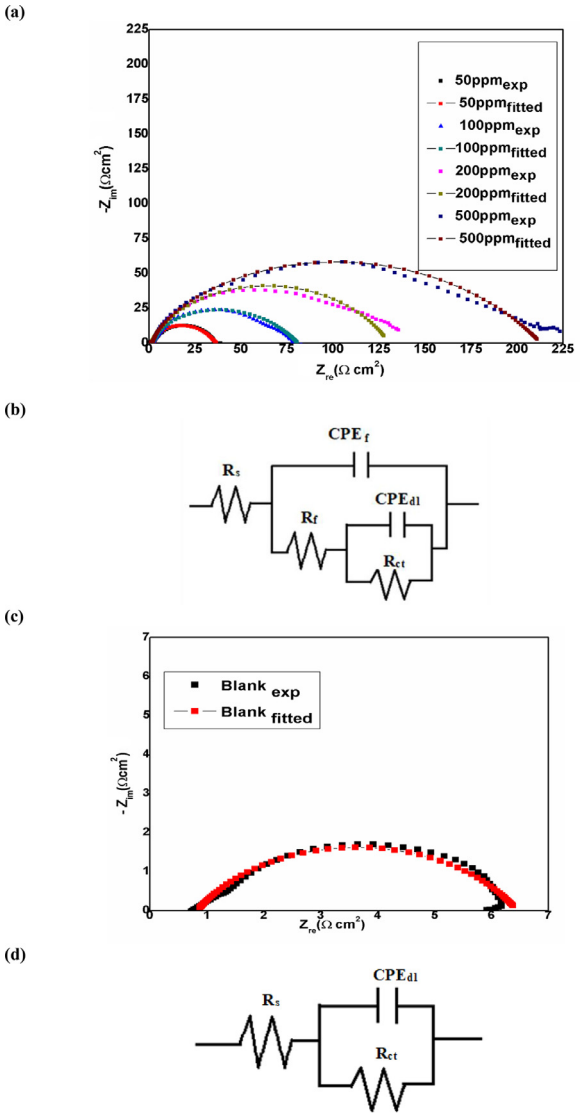

Fig. 10. **(a)** Experimental and fitted modelof MS dissolution in HCl medium with inhibitor DMPIP **(b)** Equivalent circuitof MS dissolution in HCl medium with inhibitor DMPIP **(c)** Experimental and fitted model of MS dissolution in HCl medium without inhibitor DMPIP **(d)** Equivalent circuit of MS dissolution in HCl medium without inhibitor DMPIP.

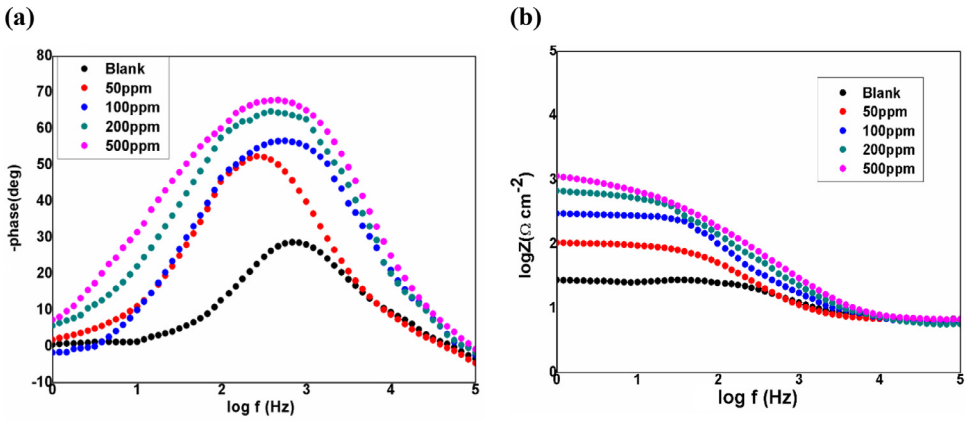

Fig. 11. **(a)** Bode phase angle plots and **(b)** Bode modulus plots for MS in 0.5 M HCl in the absence and presence of different concentrations of DMPIP inhibitor.

resistance values using the Eq. (10).

$$\eta\% = \frac{R_{ct}^{o} - R_{ct}}{R_{ct}^{o}} \times 100 \quad (10)$$

where R°_{ct} and R_{ct} are the charge transfer resistance values in the absence and presence of DMPIP. The results in Table 4 corroborate that largest inhibitory effect of DMPIP at 303 K at 500 ppm (94.85%) which is in good agreement with the Tafel extrapolation results.

There is a single peak for blank/uninhibited solution in Bode phase angle plot (Fig. 11a) shows that the electrochemical impedance measurements were fit well in one time constant equivalent circuit model and also one phase maximum in Bode Modulus plot (Fig. 11b) indicates only one relaxation process, which would be the charge transfer process taking place at the metal/electrolyte interface. For the inhibited solutions, as concentration of the inhibitor is increased, higher values of Bode phase angle and broadening of the Bode diagrams observed which reflect the formation of protective film on the MS surface due to the adsorption of inhibitor molecule which gives a more capacitive response [16,77,82].

The above electrochemical experimental results prove that the structurally modified, newly synthesized, imidazo pyridine derivative namely DMPIP shows better inhibition action (96.7%) compare to the earlier reported studies [42,43] on MS surface in 0.5 M HCl.

3.3. Surface morphological analysis

3.3.1. Scanning electron microscopy (SEM) analysis

The SEM images of the MS surface in the absence and presence of 500 ppm concentration of DMPIP in 0.5 M HCl solution exposed to 15 h were recorded. Fig. 12(a) portrays the surface image of the mirror-finished sample; Fig. 12(b) depicts the image of the sample surface is rough and damaged in aggressive media, where HCl corrodes the surface highly in the absence of DMPIP. Fig. 12(c) depicts the SEM image of mild steel sample in presence of 500 ppm of inhibitor DMPIP, shows roughness of the surface has been decreased infers the adsorption of DMPIP molecules which hampers the electrochemical reactions of the MS in HCl solution by adsorbing on the surface and decreased corrosion rate.

3.3.2. Energy-dispersive X-ray spectroscopy (EDX) analysis

EDX investigations were performed to identify the composition of MS surface in the presence and absence of DMPIP in 0.5 M HCl solution. EDX method was used to determine the percentage atomic content of various elements of the polished, MS surface with and without the presence of DMPIP. The corresponding EDX analysis of the selected areas on the SEM images as shown in Fig. 13. The EDX results showed the presence of Fe, O, Cl and C on the steel surface as shown in Table 5. The highest oxygen content was present in the uninhibited solution and also showed the chlorine peaks confirming the formation of corrosion product(iron oxide or iron chloride) on the surface of MS (Fig. 13(b)). In the case of MS coupon dipped in the corrosive media with 500 ppm of inhibitor DMPIP for 15 h, no chlorine peaks, considerable decrease in oxygen content were observed and highest carbon content seen due to the interaction of inhibitor molecule with MS surface to form the protective film, which thus reduces the corrosion rate (Fig. 13(c)).

Table 5
Percentage atomic contents of elements derived from EDX spectra.

	Fe	Si	Mn	O	C	Cl
Polished	88.94	0.88	0.71	6.16	3.08	–
Blank	51.78	0.48	0.19	43.59	2.1	0.69
DMPIP	75.38	0.69	0.44	15.62	7.8	–

3.3.3. FT-IR spectroscopic analysis

To observe the attachment of inhibitor molecules to the surface, the insoluble material formed on the surface of the corroded steel coupons were scraped, and subjected to IR spectra. FTIR spectra shows new bonding information of product formed on the steel surface with and without inhibitor.

The FTIR spectra of DMPIP inhibitor, MS sample after immersion in 0.5 M HCl and MS sample after immersion in 0.5 M HCl and 500 ppm of DMPIP inhibitor for 15 h is depicted in Fig. 14. FT-IR spectrum of the mild steel surface with inhibitor in corrosive medium shows similar FT-IR spectrum as that of inhibitor and the peak regions of the protective film are basically consistent with that of pure DMPIP inhibitor. FT-IR spectra of inhibitor shows some characteristic bands such as the band around 3246 cm^{-1} is attributed to (N–H) and band around 1664 cm^{-1} is due to (−C=O) of amide carbonyl vibration. The spectrum of DMPIP shows bands at 2806 cm^{-1} and 2903 cm^{-1} corresponding to (−C–H) aliphatic of methyl group (−CH3) of (-O-CH_3) entity. 1485 cm^{-1} of aromatic (C=C) stretching and 1533 cm^{-1} is attributed to the (-C=N) of imidazo pyridine ring. The spectrum of the absorbed DMPIP on mild steel shows remarkable change in absorption bands of functional groups of DMPIP molecule. We can clearly observe that the intensity of most bands are significantly reduced compared to spectrum of DMPIP. The wave number of the bands located at 1664 cm^{-1} and at 1533 cm^{-1} is considerably reduced to 1647 cm^{-1} and 1512 cm^{-1} suggesting that these regions are mainly involved in the adsorption through the donor-acceptor process. Indeed, the spec-

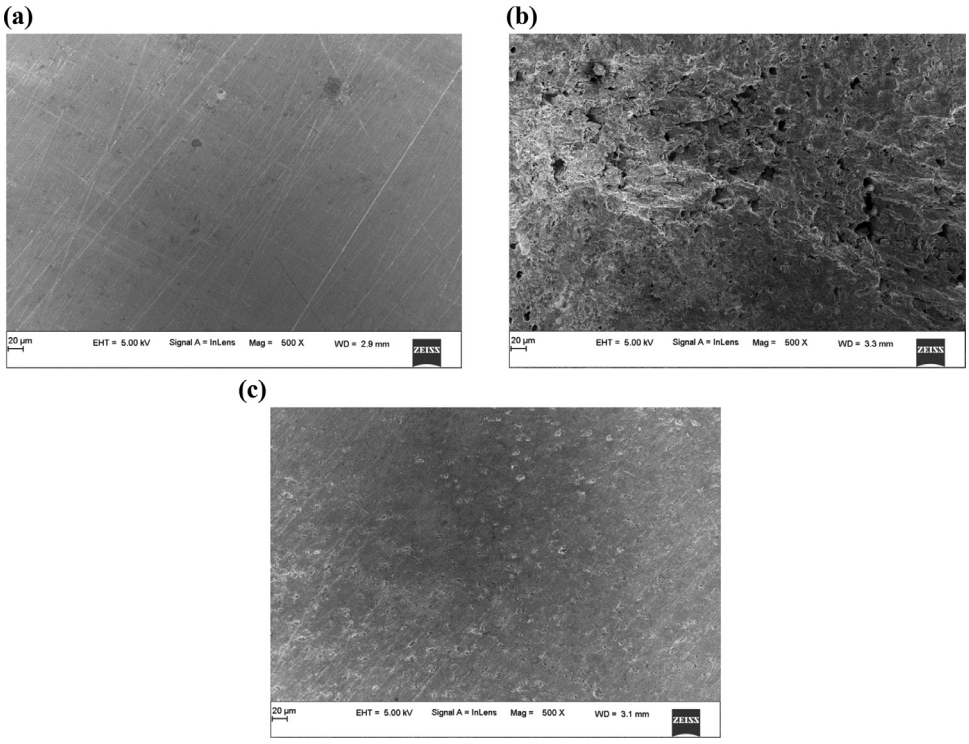

Fig. 12. SEM images of (a) Polished surface of MS, **(b)** MS surface in 0.5 M HCl without inhibitor and **(c)** MS surface in presence of 500 ppm DMPIP.

trum of adsorbed DMPIP inhibitor also shows the disappearance of bands observed at 3083 cm^{-1} associated to aromatic (C–H) and those at 3246 cm^{-1} of (–N–H) amide, suggesting the participation of these group atoms in chemical interactions with mild steel. The intensity of NH band has shifted from 3246 cm^{-1} to 3350 cm^{-1}. The wide band observed at 3350 cm^{-1} is due to the hydrogen bonding between MS surface and inhibitor molecule thus confirms the interaction between protonated inhibitor DMPIP and MS through hydrogen bonding forming protective layer on the MS surface [53,83]

4. Quantum chemical calculations

Quantum chemical calculations can accurately predict the ground state of each atom as well as molecules, the excited states and the transition states in chemical reactions. Thus, quantum chemical properties play a major role in evaluating the correlation between geometrical configuration and the inhibition efficiency. DFT calculations are extensively used by various researchers to interpret the inhibition mechanism. Quantum chemical calculations gives the reactivity indices for both neutral and protonated form of DMPIP in the aqueous phase. In the present study, experimental results are correlated and confirmed with molecular parameters such as orbital energies, dipole moment, hardness, softness, electrophilicity index, ionization potential, Mulliken distribution and Fukui indices. The optimized geometry for both neutral and protonated form of DMPIP in the aqueous phase are shown in Fig. 15.

The distribution of frontier molecular orbitals, natural atomic charge and local reactivity descriptors (Fukui indices) are considered as influencing factors to study the active sites on the inhibitors. Generally, Frontier molecular orbital theory (FMO) is considered to predict the adsorption centers of inhibitors responsible for the interaction with surface metal atoms [84]. The bonding between DMPIP and MS surface can be predicted by considering E_{HOMO} and E_{LUMO}. The HOMO (highest occupied molecular orbital) distribution characterize the nucleophilic component whereas LUMO (lowest unoccupied molecular orbital) distribution indicate electrophilic component in a molecule.

The higher HOMO energy of the molecule is responsible for the higher electron-donating ability to appropriate acceptor molecule. This explains adsorption of the DMPIP molecule on MS surface by delocalized pi electrons or by unpaired electrons present on heteroatom. The lower LUMO energy signifies the higher electron-accepting ability of a molecule [85]. ΔE_{gap} ($E_{LUMO} - E_{HOMO}$) determines the reactivity of DMPIP toward the adsorption on MS surface. A large value of ΔE_{gap} implies high chemical stability for the molecule in reactions [86]. The HOMO-LUMO electron density over protonated and neutral DMPIP molecules in the aqueous phase are presented in Fig. 16.

As seen from Fig. 16, DMPIP has different HOMO-LUMO electron density in the protonated and neutral forms of DMPIP. The populations of HOMO densities are focused on imidazo pyridine ring having nitrogen atoms in protonated form, while the neutral form has the HOMO densities mainly around dimethoxy substituted benzene moiety. The LUMO distributions are, however, found all over the imidazo pyridine ring as well as dimethoxy substituted benzene ring for the protonated form but in the neutral form, it is more distributed in imidazo pyridine ring.

The protonated form of the DMPIP donates electrons to the unoccupied *d* orbitals of iron atom to form coordination bond. In neutral form, a back-donating bond is preferred by DMPIP molecule by accepting the electrons from anti-bonding orbitals of the iron atom [87].

From Table 6, it is evident that DMPIP has high E_{HOMO} in protonated form than in neutral form, suggesting weaker electron donation ability in neutral form compared to protonated form. It can also be observed that the neutral form of DMPIP shows the lowest E_{LUMO} value, making the neutral form most likely to have interactions with the mild steel. The calculations further show that the protonated form has lower ΔE_{gap}value (1.712 eV), indicating that DMPIP in protonated form is the most reactive formwhich can be

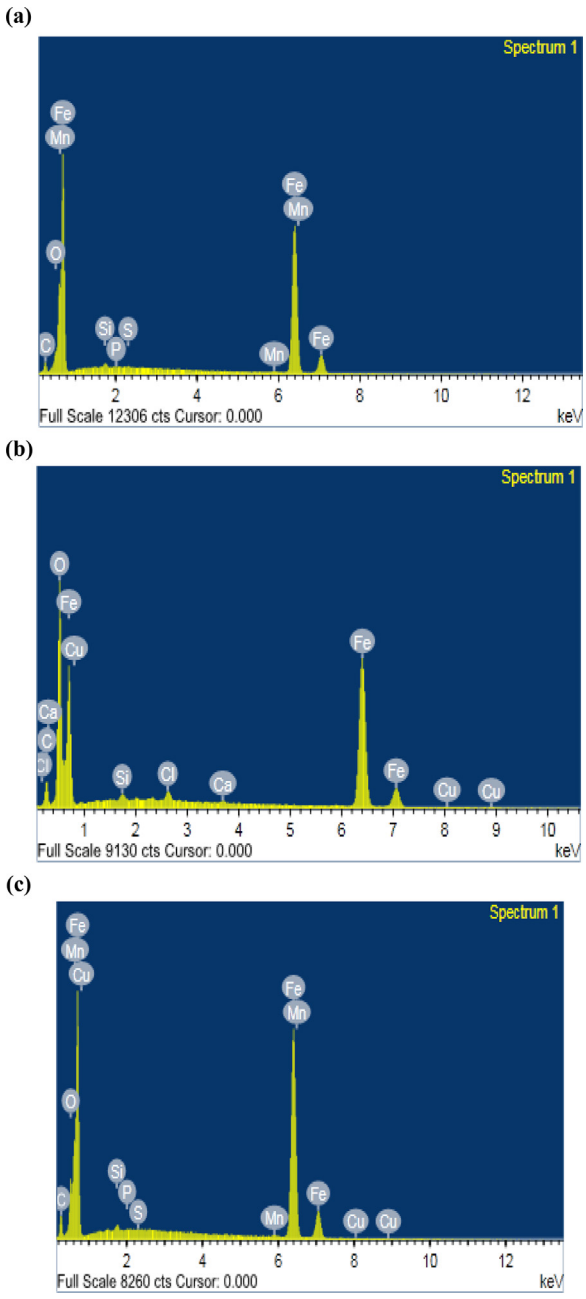

Fig. 13. **(a)** EDX spectra of polished MS, **(b)** EDX spectra of MS in 0.5 M HCl and **(c)** EDX spectra of MS in presence of 500 ppm of DMPIP.

Table 6
B3LYP/6–311++*G* (d, p) level.

Quantum chemical parameters	Aqueous phase	
	Neutral form	Protonated form
Total energy, ΔE_T (au)	−3673.29	−3676.49
E_{HOMO} (eV)	−5.826	−3.499
E_{LUMO} (eV)	−2.061	−1.787
ΔE_{gap} (eV)	3.764	1.712
Dipole moment (D)	8.955	9.022
Ionization potential, I (eV)	5.825	3.499
Electron affinity, A (eV)	2.061	1.787
Electronegativity (χ)	3.943	2.643
Hardness (η)	1.882	0.856
Softness (σ)	0.5313	1.168
Fraction of electrons transferred (ΔN)	0.81	2.544
Electrophilicity, ω (D^2/eV)	21.28	47.85

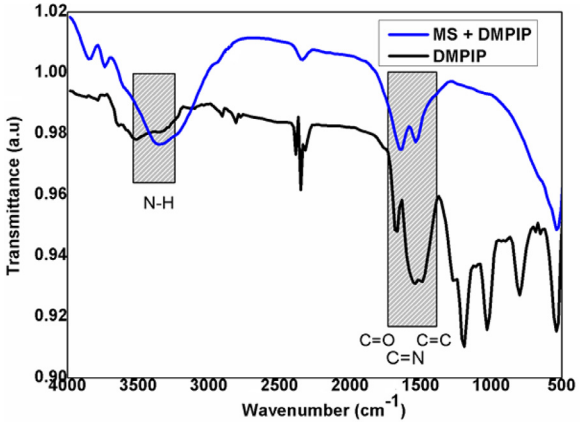

Fig. 14. FT-IR spectra of DMPIP and MS in 0.5 M HCl with 500 ppm of inhibitor.

easily adsorbed on MS surface effecting higher surface coverage. This fact correlates well with the experimental data, which shows the protonated form of inhibitor interacts with MS through electrostatic interaction. Thus, the strong interaction between the cationic form of DMPIP and empty *d*-orbital of the iron atom substantially enhanced the inhibitive action of DMPIP on MS surface through physisorption [85]. Also, DMPIP adsorption on the MS surface by the neutral form of DMPIP is possible in the overall inhibition process.

The molecular descriptors such as ΔE_{gap}(Energy Gap), I (Ionization energy), A (Electron Affinity), μ (Dipole Moment), χ (Absolute Electronegativity), η (hardness), σ (Softness), ω (electrophilicity index) and ΔN (Fraction) are calculated using following equations [66]:

$$\Delta E\ (Energy\ Gap) = E_{LUMO} - E_{HOMO} \tag{11}$$

$$I\ (Ionization\ Potential) = -E_{HOMO} \tag{12}$$

$$A\ (Electron\ Affinity) = -E_{LUMO} \tag{13}$$

$$\chi\ (Absolute\ electronegativity) = \frac{(I+A)}{2} = -\frac{(E_{HOMO} + E_{LUMO})}{2} \tag{14}$$

$$\eta\ (hardness) = \frac{(I-A)}{2} = -\frac{(E_{HOMO} - E_{LUMO})}{2} \tag{15}$$

$$\sigma\ (softness) = \frac{1}{hardness} \tag{16}$$

$$\omega\ (electrophilicity\ index) = \frac{\mu^2}{2\eta} \tag{17}$$

$$\Delta N\ (Fraction) = \frac{(\chi Fe - \chi inhibitor)}{2(\eta Fe + \eta inhibitor)} \tag{18}$$

Dipole moment is one of the major electronic parameters to evaluate the intermolecular interactions like dipole-dipole interaction, van der Waals interactions etc. From Table 6, it is found that the dipole moment for DMPIP molecule (8.955 debye) is higher compared to the dipole moment of water (1.85 debye) proves DMPIP has higher propensity to adsorb on MS surface than already existing water molecules. A large dipole moment makes the molecule more polar, which helps to adsorb on MS surface, increasing the inhibition efficiency [88]. Consequently, the reaction

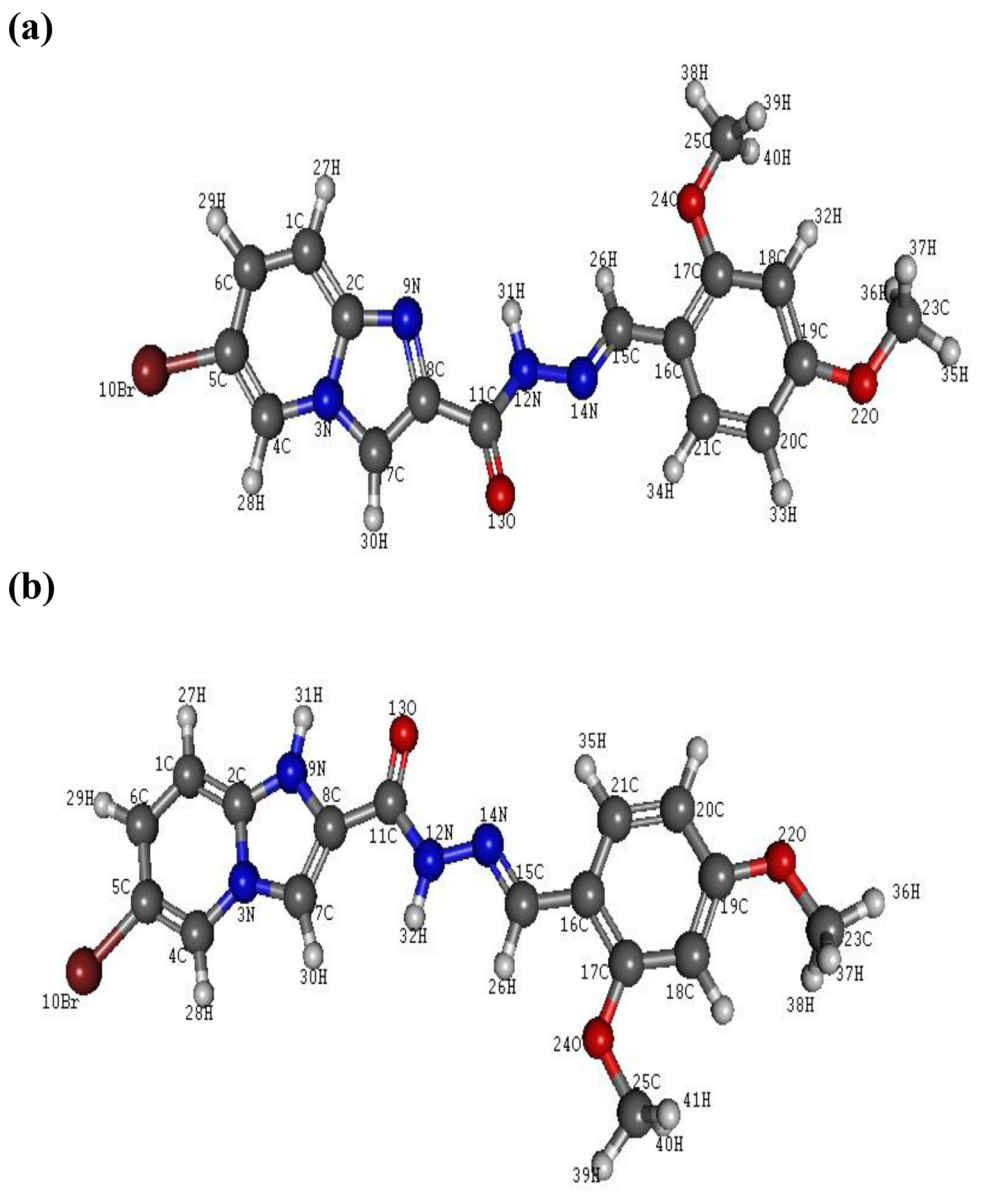

Fig. 15. Optimized geometry for DMPIP molecule obtained by DFT at B3LYP/6–311++*G*(d, p) level in **(a)** neutral and **(b)** protonated form in aqueous phase.

between the charged sites on the DMPIP and MS results in electrostatic dipole-dipole interaction. Thus, the correlation between the dipole moment and inhibition efficiency of the inhibitor suggests the process of physical adsorption [89] of DMPIP on the MS surface, as revealed experimentally. Besides, higher μ increases the volume of the inhibitor, thereby increasing the contact area between the DMPIP and the MS surface for adsorption phenomenon [90]. Thus, a higher dipole moment enhances the corrosion inhibition ability of the inhibitor.

Absolute hardness and softness measure the chemical reactivity and kinetic stability of the molecule to a great extent. According to Pearson, hard molecules with large E_{gap} cannot yield good corrosion inhibition efficiency [91]. A soft molecule has a small energy gap, and a hard molecule has a large energy gap [92]. Since Fe metal atoms are considered as soft acids, according to HSAB theory, the inhibitor molecules should possess larger softness and lower hardness value to interact and get adsorbed on the metal surface more easily than the hard molecules. Soft molecules are more reactive because they can easily provide electrons to an acceptor molecule due small energy gap. It is found that the protonated form of DMPIP has the lowest hardness, lowest ΔE_{gap} and the highest softness, making the moiety more reactive. This manifests a better inhibitive performance of DMPIP in the protonated cationic form through electrostatic attraction between inhibitor molecule and mild steel vacant *d* orbital (physisorption). This agrees well with the obtained experimental results.

The fraction of electrons transferred from DMPIP to the mild steel surface is denoted as, ΔN [93]. NuhaWazzen et al. [94] explain that when $\Delta N > 0$, higher the electron transfer from the inhibitor to mild steel and when $\Delta N < 0$, the transfer of electrons from the inhibitor to metal is low. When $\Delta N < 3.6$, the electron-donating capability of the inhibitor molecule to metal surface increases which enhance the inhibition efficiency of molecule. ΔN values show that the inhibition effect results due to the donation of the electrons [95,96]. ΔN values for the inhibitor in both neutral and protonated found to be much lesser than 3.6, thus making inhibitor DMPIP as electron donor and mild steel surface as the acceptor of electrons.

The global electrophilicity index (ω) specifies the potential of the inhibitor to withdraw the electrons from the metal atom [97].

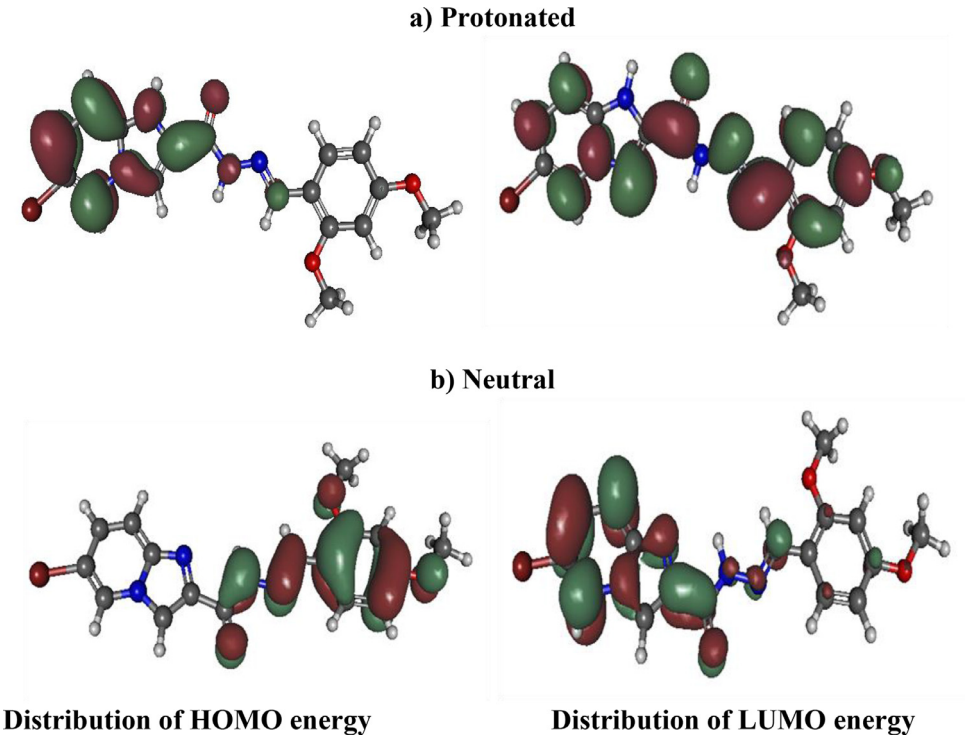

Fig. 16. HOMO-LUMO energy distribution over DMPIP molecule by B3LYP/6–311++*G* (d, p) level in aqueous phase **(a)** protonated and **(b)** neutral molecule.

It has been reported that the higher the value of ω, the superior is the ability to withdraw the electrons [47,98]. The protonated form of DMPIP molecule has high ω value compared to the neutral form and in addition, shows the highest ability to accept electrons from the mild steel. This attributes to the formation of back donating bond where the inhibitor receives electrons from the iron atom along with the formation of coordination bond between the unoccupied/ empty *d*-orbitals of the metal atom and the inhibitor molecule. The process of donation and back-donation fortify the adsorption of DMPIP onto the mild steel surface [85]; thereby increasing the adsorption ability of the inhibitor molecule on the mild steel surface.

The change in total energy (ΔE_T) is associated with the adsorption process which describes the energy change associated with the donation and back-donation processes occurring between the inhibitor and metal [94,99,100]. From Table 5, it can be seen that $\eta > 0$ and $\Delta E_T < 0$ for both protonated and neutral form of DMPIP in the aqueous phase. This result suggests the charge transfer to DMPIP molecule accompanied by back-donation process is energetically favorable [89]. Anyhow it is essential to note that the back-donation process occurs is not completely predicted by ΔE_T values acquired. It shows whether both the processes (charge transfer to the inhibitor and back donation from the inhibitor) occur in the inhibition mechanism. Also, the change in energy is directly proportional to the absolute hardness of the molecule.

4.1. Mulliken population analysis

Further, Mulliken population analysis was carried out to predict the adsorption site of the inhibitor molecule for both neutral and protonated forms of DMPIP to analyze the factor of anti-corrosive properties of DMPIP for MS in hydrochloric acid medium. Fig. 17 shows the Mulliken atomic charges calculated for neutral and protonated form of DMPIP in aqueous phase. It is reported that more negative the atomic charge of the inhibitor molecule, more efficiently the atom donates its electrons to the unoccupied orbital of the metal atom by forming donor-acceptor interaction [101].

From Fig. 17, it can be noted that most of the nitrogen atoms, oxygen atoms as well as some carbon atoms carry negative charge centers. These charge centers share the electrons to the metal to form a coordinate bond. Some of the carbon atoms are electron deficient with high positive charge due to the delocalization of electron on the system. It should be noted that the neutral form of the DMPIP inhibitor has more negative charge centers compared to the protonated form which boosts its adsorption process and increases the corrosion-inhibiting properties. Further, the total negative charge values of the common heteroatoms are smaller in case of protonated forms compare to the neutral forms. Thus, the protonation process decreases the adsorption strength of the molecule through its active adsorption sites on the mild steel surface. In aqueous solution for the neutral form, the total negative charge measured from the partial Mulliken charges on the heteroatoms nitrogen and oxygen gives the information about the active centers present on the inhibitor which interacts with the mild steel surface. More negatively charged atom, its tendency to donate electrons increases [89]. 3N, 9N, 12N, and 13O (Fig. 17(b)) are the negatively charged centers in neutral form, indicating these are the active sites interact with steel, get adsorbed on mild steel surface.

4.2. Fukui indices

To analyze the behavior of the different site, it is essential to consider local reactivity descriptors like the Fukui function [102,103] which demonstrate the reactivity of the frontier molecular orbitals. The $fk^+$and fk^-were calculated to predict the most probable atomic sites for nucleophilic and electrophilic attack respectively. Table 7shows the values of natural population (P (N), P (N-1), and P ($N + 1$)) with the corresponding Fukui functions (fk^+, $fk^-$and fk°) values of the inhibitor, DMPIP. The electrophilic and nucleophilic Fukui functions for a site in a molecule can be

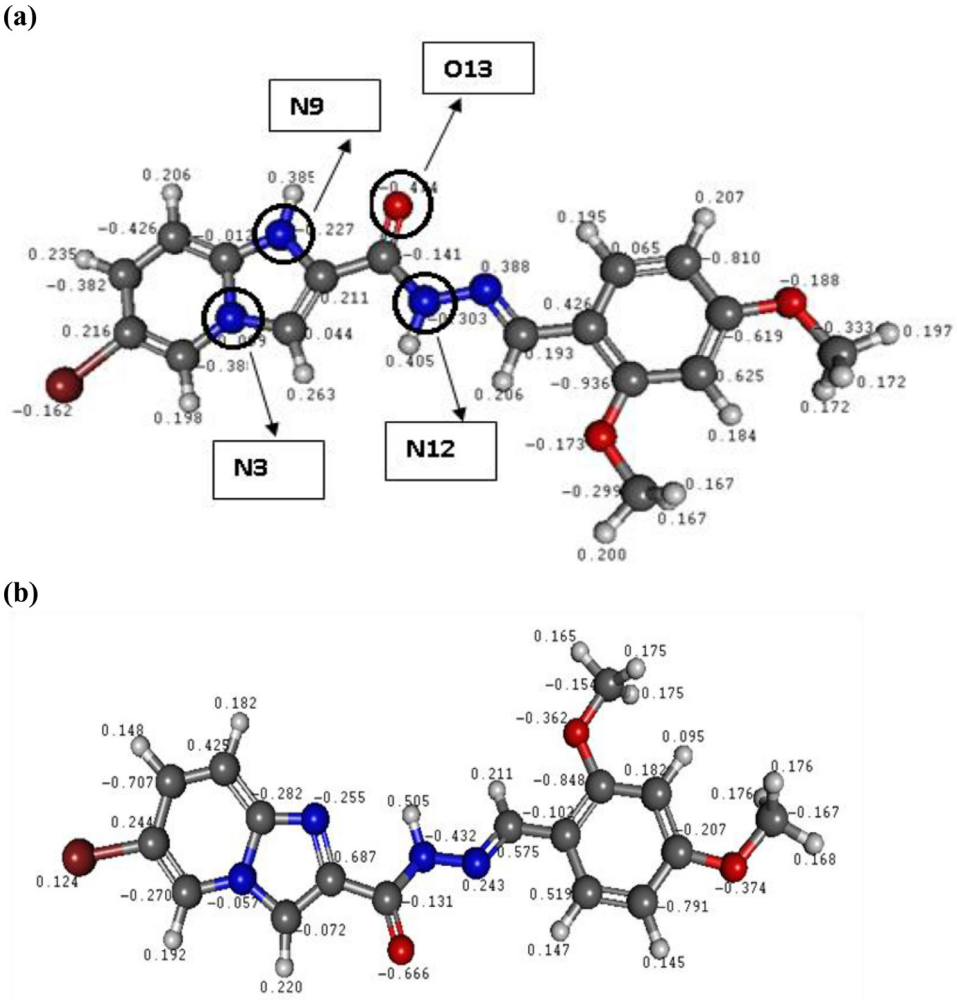

Fig. 17. Mulliken charge distribution for DMPIP molecule at B3LYP/6–311++*G* (d, p) level **(a)** protonated form and **(b)** neutral form.

Table 7
Calculated Mulliken charges and Fukui indices for heteroatoms of DMPIP using B3LYP/6–311++*G* (d, p) basis Set.

				Fukui indices		
	Anion qk($N+1$)	cation qk(N-1)	neutral qkN	Nucleophilic fk^+	electrophilic fk^-	Radical fk°
3N	0.122411	0.013366	−0.05671	0.179121	−0.070076	0.054523
9N	−0.18264	0.066638	−0.25462	0.071979	−0.321255	−0.12464
12N	−0.21323	0.131489	−0.43227	0.21904	−0.563763	−0.17236
14N	0.226147	0.187015	0.242675	−0.016528	0.05566	0.019566
13O	−0.58011	0.094634	−0.66619	0.08608	−0.760821	−0.33737

determined by following equations [87]:

$$\text{Nucleophilic attack}: f+(\mathrm{r}) = \rho\, N+1(\mathrm{r}) - \rho\, \mathrm{N}\,(\mathrm{r}) \quad (19)$$

$$\text{Electrophilic attack}: f-(\mathrm{r}) = \rho\, \mathrm{N}\,(\mathrm{r}) - \rho\, N-1(\mathrm{r}) \quad (20)$$

$$\text{Radical attack}: \mathrm{f(r)} = 1/2(\rho\mathrm{N}+1(\mathrm{r}) - \rho\mathrm{N}-1(\mathrm{r})) \quad (21)$$

Where ρN represents the density of electron around the molecule at a point *r*. The number of electrons, *N*, $N+1$ and $N+2$, corresponds to neutral molecule, anion (addition of an electron to the LUMO of the neutral molecule) and cation (removal of an electron from the HOMO of the neutral molecule) respectively. Nitrogen atoms (3 $N = -0.070$ and 14 $N = 0.056$) with highest values of $fk^-$are the most susceptible sites for electrophilic attacks. In the same vein, sites (3 $N = 0.179$ and 12 $N = 0.219$) with highest values of $fk^+$are the most vulnerable sites for nucleophilic attacks.

5. Conclusion

A new N-heterocyclic compound DMPIP was synthesized and its inhibition ability on corrosion of MS in 0.5 M HCl was investigated and correlated with the quantum chemical calculations.

DMPIP acts as a potential corrosion inhibitor for MS in hydrochloric acid medium and its inhibition efficiency increases as the concentration of the additive were increased but with the rise in temperature corrosion rate increases. Potentiodynamic polarization curves demonstrated that DMPIP act as a mixed-type inhibitor suppressing both metal dissolution and hydrogen evolution reaction rates. EIS plots in the presence of DMPIP showed two capac-

itive loops associated with the formation of protective film due to the accumulation of inhibitors at the steel surface. The decreased CPE_{dl} values and increased R_{ct} values were attributed to the decreased local dielectric constant or increased thickness of electrical double layer of the protective film. The adsorption of DMPIP molecules on the MS surface was described by Langmuir adsorption isotherm with a high correlation coefficient. The polarization and impedance spectroscopic studies were in good agreement with each other. Activation and thermodynamic data suggested that the adsorption mechanism of DMPIP on MS surface in 0.5 M HCl solution was mainly through physisorption. The SEM micrographs and EDX data confirmed that DMPIP molecules form an efficient protective layer on the MS surface. Further, FT-IR spectroscopic analysis confirmed the inhibitonary act of DMPIP molecules on MS surface. Data obtained from quantum chemical calculations using DFT at the B3LYP/6–311++G(d,p) level of theory were correlated to the inhibitive effect of inhibitor. Protonation of DMPIP results in the formation of Fe-DMPIP complexes, with higher complexation energy than the deprotonated form, which leads to a greater reactivity. The findings of theoretical calculations were in good agreement with the experimental ones.

Declaration of Competing Interest

The authors declare that they have no known competing financial interests or personal relationships that could have appeared to influence the work reported in this paper.

CRediT authorship contribution statement

K Vranda Shenoy: Methodology, Validation, Formal analysis, Investigation, Writing - original draft, Visualization. **Pushyaraga P Venugopal:** Software, Methodology, Validation, Formal analysis, Writing - original draft, Visualization. **P D Reena Kumari:** Conceptualization, Methodology, Formal analysis, Resources, Writing - review & editing, Supervision. **Debashree Chakraborty:** Formal analysis, Resources, Writing - review & editing, Supervision, Funding acquisition.

Acknowledgement

Funding from DST, SERB (CRG/2019/000578) is highly acknowledged. We would like to thank Department of Chemistry and Department of Physics, NITK Surathkal for their constant support.

Supplementary materials

Supplementary material associated with this article can be found, in the online version, at doi:10.1016/j.molstruc.2021.130074.

References

[1] B. El Ibrahimi, A. Jmiai, K. El Mouaden, A. Baddouh, S. El Issami, L. Bazzi, M. Hilali, Effect of solution's PH and molecular structure of three linear α-amino acids on the corrosion of tin in salt solution: a combined experimental and theoretical approach, J. Mol. Struct. 1196 (2019) 105–118, doi:10.1016/j.molstruc.2019.06.072.

[2] B. EL Ibrahimi, L.;. Bazzi, S. EL Issami, The role of PH in corrosion inhibition of tin using the proline amino acid: theoretical and experimental investigations, RSC Adv. 10 (50) (2020) 29696–29704, doi:10.1039/D0RA04333H.

[3] T. Peme, L.O. Olasunkanmi, I. Bahadur, A.S. Adekunle, M.M. Kabanda, E.E. Ebenso, Adsorption and corrosion inhibition studies of some selected dyes as corrosion inhibitors for mild steel in acidic medium: gravimetric, electrochemical, quantum chemical studies and synergistic effect with iodide ions, Mol. Basel Switz. 20 (9) (2015) 16004–16029, doi:10.3390/molecules200916004.

[4] R. Aslam, M. Mobin, I.B. Huda; Obot, A.H. Alamri, Ionic liquids derived from α-amino acid ester salts as potent green corrosion inhibitors for mild steel in 1M HCl, J. Mol. Liq. 318 (2020) 113982, doi:10.1016/j.molliq.2020.113982.

[5] M.H. Sliem, M. Afifi, A. Bahgat Radwan, E.M. Fayyad, M.F. Shibl, F.E.-T. Heakal, A.M. Abdullah, AEO7 Surfactant as an eco-friendly corrosion inhibitor for carbon steel in HCl solution, Sci. Rep. 9 (1) (2019) 2319, doi:10.1038/s41598-018-37254-7.

[6] J. Aslam, Cationic gemini surfactant as corrosion inhibitor for mild steel in 1M HCl and synergistic effect of organic salt (Sodium Tosylate), J. Adhes. Sci. Technol. 33 (18) (2019) 1989–2009, doi:10.1080/01694243.2019.1617227.

[7] M. Mobin, R. Aslam, J. Aslam, Synergistic effect of cationic gemini surfactants and butanol on the corrosion inhibition performance of mild steel in acid solution, Mater. Chem. Phys. 223 (2019) 623–633, doi:10.1016/j.matchemphys.2018.11.032.

[8] A. Biswas, S. Pal, G. Udayabhanu, Experimental and theoretical studies of xanthan gum and its graft co-polymer as corrosion inhibitor for mild steel in 15% HCl, Appl. Surf. Sci. 353 (2015) 173–183, doi:10.1016/j.apsusc.2015.06.128.

[9] S.A. Umoren, M.J. Banera, T. Alonso-Garcia, C.A. Gervasi, M.V. Mirífico, Inhibition of mild steel corrosion in HCl solution using Chitosan, Cellulose 20 (5) (2013) 2529–2545, doi:10.1007/s10570-013-0021-5.

[10] R. Sadeghi Erami, M. Amirnasr, S. Meghdadi, M. Talebian, H. Farrokhpour, K. Raeissi, Carboxamide derivatives as new corrosion inhibitors for mild steel protection in hydrochloric acid solution, Corros. Sci. 151 (2019) 190–197, doi:10.1016/j.corsci.2019.02.019.

[11] M.I. Awad, Eco friendly corrosion inhibitors: inhibitive action of quinine for corrosion of low carbon steel in 1m HCl, J. Appl. Electrochem. 36 (10) (2006) 1163–1168, doi:10.1007/s10800-006-9204-1.

[12] H. Elmsellem, M.H. Youssouf, A. Aouniti, T. Ben Hadda, A. Chetouani, B. Hammouti, Adsorption and inhibition effect of curcumin on mild steel corrosion in hydrochloric acid, Russ. J. Appl. Chem. 87 (6) (2014) 744–753, doi:10.1134/S1070427214060147.

[13] X. Luo, C. Ci, J. Li, K. Lin, S. Du, H. Zhang, X. Li, Y.F. Cheng, J. Zang, Y. Liu, 4-Aminoazobenzene modified natural glucomannan as a green eco-friendly inhibitor for the mild steel in 0.5M HCl solution, Corros. Sci. 151 (2019) 132–142, doi:10.1016/j.corsci.2019.02.027.

[14] P. Roy, P. Karfa, U. Adhikari, D. Sukul, Corrosion inhibition of mild steel in acidic medium by polyacrylamide grafted guar gum with various grafting percentage: effect of intramolecular synergism, Corros. Sci. 88 (2014) 246–253, doi:10.1016/j.corsci.2014.07.039.

[15] M. Ramezanzadeh, G. Bahlakeh, Z. Sanaei, B. Ramezanzadeh, Corrosion inhibition of mild steel in 1M HCl solution by ethanolic extract of eco-friendly mangifera indica (mango) leaves: electrochemical, molecular dynamics, Monte Carlo and ab initio study, Appl. Surf. Sci. 463 (2019) 1058–1077, doi:10.1016/j.apsusc.2018.09.029.

[16] M. Ramezanzadeh, G. Bahlakeh, B. Ramezanzadeh, Study of the synergistic effect of mangifera indica leaves extract and zinc ions on the mild steel corrosion inhibition in simulated seawater: computational and electrochemical studies, J. Mol. Liq. 292 (2019) 111387, doi:10.1016/j.molliq.2019.111387.

[17] Z. Sanaei, M. Ramezanzadeh, G. Bahlakeh, B. Ramezanzadeh, Use of Rosa Canina fruit extract as a green corrosion inhibitor for mild steel in 1M HCl solution: a complementary experimental, molecular dynamics and quantum mechanics investigation, J. Ind. Eng. Chem. 69 (2019) 18–31, doi:10.1016/j.jiec.2018.09.013.

[18] A. Dehghani, G. Bahlakeh, B. Ramezanzadeh, M. Ramezanzadeh, A combined experimental and theoretical study of green corrosion inhibition of mild steel in HCl solution by aqueous citrullus lanatus fruit (CLF) extract, J. Mol. Liq. 279 (2019) 603–624, doi:10.1016/j.molliq.2019.02.010.

[19] P. Roy, T. Maji, S. Dey, D. Sukul, Adsorption behaviour of gluten hydrolysate on mild steel in 1M HCl and its role as a green corrosion inhibitor, RSC Adv. 5 (75) (2015) 61170–61178, doi:10.1039/C5RA12266J.

[20] T. Rabizadeh, S.K. Asl, Casein as a natural protein to inhibit the corrosion of mild steel in HCl solution, J. Mol. Liq. 276 (2019) 694–704, doi:10.1016/j.molliq.2018.11.162.

[21] E. Özdemir, G. Gece, A theoretical investigation of some N-hydroxymethyl amino acids as corrosion inhibitors for mild steel, Key Eng. Mater. 800 (2019) 108–112, doi:10.4028/www.scientific.net/KEM.800.108.

[22] S. Satpati, S.Kr. Saha, A. Suhasaria, P. Banerjee, D Sukul, Adsorption and anti-corrosion characteristics of vanillin Schiff bases on mild steel in 1M HCl: experimental and theoretical study, RSC Adv. 10 (16) (2020) 9258–9273, doi:10.1039/C9RA07982C.

[23] A.E. Aatiaoui, M. Koudad, T. Chelfi, S. Erkan, M. Azzouzi, A. Aouniti, K. Savaş, M. Kaddouri, N. Benchat, A. Oussaid, Experimental and theoretical study of new schiff bases based on imidazo(1,2-a)pyridine as corrosion inhibitor of mild steel in 1M HCl, J. Mol. Struct. 1226 (2021) 129372, doi:10.1016/j.molstruc.2020.129372.

[24] B. El Ibrahimi, K. El Mouaden, A. Jmiai, A. Baddouh, S. El Issami, L. Bazzi, M. Hilali, Understanding the influence of solution's PH on the corrosion of tin in saline solution containing functional amino acids using electrochemical techniques and molecular modeling, Surf. Interfaces 17 (2019) 100343, doi:10.1016/j.surfin.2019.100343.

[25] B. Ibrahimi, A. Jmiai, A. Somoue, R. Oukhrib, Cysteine duality effect on the corrosion inhibition and acceleration of 3003 aluminium alloy in a 2% NaCl solution: *port*, Electrochim. Acta 36 (6) (2018) 403–422, doi:10.4152/pea.201806403.

[26] S.K. Ahmed, W.B. Ali, A.A. Khadom, Synthesis and investigations of heterocyclic compounds as corrosion inhibitors for mild steel in hydrochloric acid, Int. J. Ind. Chem. 10 (2) (2019) 159–173, doi:10.1007/s40090-019-0181-8.

[27] G. Palanisamy, Corrosion inhibitors, in: A. Singh (Ed.), Corrosion Inhibitors, IntechOpen, 2019, doi:10.5772/intechopen.80542.

[28] F. Bentiss, M. Traisnel, M. Lagrenee, The substituted 1,3,4-oxadiazoles: a new class of corrosion inhibitors of mild steel in acidic media, Corros. Sci. 42 (1) (2000) 127–146, doi:10.1016/S0010-938X(99)00049-9.
[29] A. Gueiffier, S. Mavel, M. Lhassani, A. Elhakmaoui, R. Snoeck, G. Andrei, O. Chavignon, J.-.C. Teulade, M. Witvrouw, J. Balzarini, E. De Clercq, J.-.P. Chapat, Synthesis of imidazo[1,2- *a*]pyridines as antiviral agents, J. Med. Chem. 41 (25) (1998) 5108–5112, doi:10.1021/jm981051y.
[30] Y. Rival, G. Grassy, A. Taudou, R. Ecalle, Antifungal activity in vitro of some imidazo[1,2-a]pyrimidine derivatives, Eur. J. Med. Chem. 26 (1) (1991) 13–18, doi:10.1016/0223-5234(91)90208-5.
[31] Y. Rival, G. Grassy, G. Michel, Synthesis and antibacterial activity of some imidazo(1,2-a)pyrimidine derivatives, Chem. Pharm. Bull. (Tokyo) 40 (5) (1992) 1170–1176, doi:10.1248/cpb.40.1170.
[32] L. Almirante, L. Polo, A. Mugnaini, E. Provinciali, P. Rugarli, A. Biancotti, A. Gamba, W. Murmann, Derivatives of imidazole. I. Synthesis and reactions of imidazo[1,2-α]pyridines with analgesic, antiinflammatory, antipyretic, and anticonvulsant activity, J. Med. Chem. 8 (3) (1965) 305–312, doi:10.1021/jm00327a007.
[33] T.H. Al-Tel, R.A. Al-Qawasmeh, R Zaarour, Design, synthesis and in vitro antimicrobial evaluation of novel imidazo[1,2-a]pyridine and imidazo[2,1-b][1,3]benzothiazole motifs, Eur. J. Med. Chem. 46 (5) (2011) 1874–1881, doi:10.1016/j.ejmech.2011.02.051.
[34] Bhatt, A.; Singh, R.K.; Kant, R. Synthesis of novel imidazo [1,2-b] pyridazine derivatives and study of their biomedicinal efficacy. 2016, 7.
[35] P.C. Lima, M.A. Avery, B.L. Tekwani, H. Alves, M. de, E.J. Barreiro, C.A.M. Fraga, Synthesis and biological evaluation of new imidazo[1,2-a]pyridine derivatives designed as mefloquine analogues, Il Farm 57 (10) (2002) 825–832, doi:10.1016/S0014-827X(02)01304-6.
[36] N. Al-lami, K.J. Salom, Pharmacological studies on some new 3- cyclic oxazepine-2- aryl imidazo(1,2-a)pyridine derivatives, J. Pharm. Sci. 11 (2019) 7.
[37] S. Ulloora, R. Shabaraya, A.V. Adhikari, New 6-bromoimidazo[1,2-a]pyridine-2-carbohydrazide derivatives: synthesis and anticonvulsant studies, Med. Chem. Res. 23 (6) (2014) 3019–3028, doi:10.1007/s00044-013-0887-7.
[38] C. Verma, M.A. Quraishi, Adsorption behavior of 8,9-bis(4 (dimethyl amino)phenyl)benzo[4,5]imidazo[1,2-a]pyridine-6,7-dicarbonitrile on mild steel surface in 1M HCl, J. Assoc. Arab Univ. Basic Appl. Sci. 22 (1) (2017) 55–61, doi:10.1016/j.jaubas.2016.01.003.
[39] Bourichi, S.; Rodi, Y.K.; Azzouzi, M.E.; Kharbach, Y.; Chahdi, F.O.; Aouniti, A. Inhibitive effect of new synthetized imidazopyridine derivatives for the mild steel corrosion in hydrochloric acid medium. 2017, 12.
[40] Salim, R.; Chihbi, E.E.; Oudda, H.; ELAoufir, Y.; El-Hajjaji, F.; Elaatiaoui, A.; Oussaid, A.; Hammouti, B.; Elmsellem, H.; Taleb, M. The inhibition effect of imidazopyridine derivatives on C38 steel in hydrochloric acid solution. 2016, 14.
[41] E. Ech-chihbi, A. Nahlé, R. Salim, H. Oudda, F. El Hajjaji, F. El Kalai, A. El Aatiaoui, M. Taleb, An investigation into quantum chemistry and experimental evaluation of imidazopyridine derivatives as corrosion inhibitors for C-steel in acidic media, J. Bio- Tribo-Corros. 5 (1) (2019) 24, doi:10.1007/s40735-019-0217-9.
[42] M. Yadav, D. Behera, S. Kumar, Experimental and theoretical investigation on adsorption and corrosion inhibition properties of imidazopyridine derivatives on mild steel in hydrochloric acid solution: corrosion inhibition of mild steel in hydrochloric acid solution, Surf. Interface Anal. 46 (9) (2014) 640–652, doi:10.1002/sia.5641.
[43] K. Bouhrira, F. Ouahiba, D. Zerouali, B. Hammouti, M. Zertoubi, N. Benchat, The inhibitive effect of 2-phenyl-3-nitroso-imidazo [1, 2-a]pyridine on the corrosion of steel in 0.5M HCl acid solution, E-J. Chem. 7 (s1) (2010) S35–S42, doi:10.1155/2010/525606.
[44] K.S. Vranda, P.D.R. Kumari, Corrosion Inhibition of Mild Steel by 6-Bromo-(4,5-Dimethoxy-2-Nitrophenyl)Methylidene]Imidazo[1,2-a]Pyridine-2-Carbohydrazide in 0.5M Hydrochloric Acid Solution, 2020 Mangalore, Indiap 040006, doi:10.1063/5.0009172.
[45] L. Li, M. Mahmoodian, C.-.Q. Li, D. Robert, Effect of corrosion and hydrogen embrittlement on microstructure and mechanical properties of mild steel, Constr. Build. Mater. 170 (2018) 78–90, doi:10.1016/j.conbuildmat.2018.03.023.
[46] C. Lee, W. Yang, R.G. Parr, Development of the colle-salvetti correlation-energy formula into a functional of the electron density, Phys. Rev. B 37 (2) (1988) 785–789, doi:10.1103/PhysRevB.37.785.
[47] R. Ditchfield, W.J. Hehre, J.A. Pople, Self-consistent molecular-orbital methods. IX. An extended Gaussian-type basis for molecular-orbital studies of organic molecules, J. Chem. Phys. 54 (2) (1971) 724–728, doi:10.1063/1.1674902.
[48] Reena Kumari, P. D., D Kumari, Experimental and theoretical evaluation of rutin as eco-friendly corrosion inhibitor for aluminum 6063 alloy in acidic medium, J. Fail. Anal. Prev. 18 (4) (2018) 856–867, doi:10.1007/s11668-018-0473-x.
[49] P. Preethi Kumari, P. Shetty, S.A. Rao, electrochemical measurements for the corrosion inhibition of mild steel in 1M hydrochloric acid by using an aromatic hydrazide derivative, Arab. J. Chem. 10 (5) (2017) 653–663, doi:10.1016/j.arabjc.2014.09.005.
[50] M. Yadav, D. Behera, S. Kumar, R.R. Sinha, Experimental and quantum chemical studies on the corrosion inhibition performance of benzimidazole derivatives for mild steel in HCl, Ind. Eng. Chem. Res. 52 (19) (2013) 6318–6328, doi:10.1021/ie400099q.
[51] M. Yadav, D. Behera, S. Kumar, Experimental and theoretical investigation on adsorption and corrosion inhibition properties of imidazopyridine derivatives on mild steel in hydrochloric acid solution: corrosion inhibition of mild steel in hydrochloric acid solution, Surf. Interface Anal. 46 (9) (2014) 640–652, doi:10.1002/sia.5641.
[52] E.S. Ferreira, C. Giacomelli, F.C. Giacomelli, A. Spinelli, Evaluation of the inhibitor effect of L-ascorbic acid on the corrosion of mild steel, Mater. Chem. Phys. 83 (1) (2004) 129–134, doi:10.1016/j.matchemphys.2003.09.020.
[53] M. Keramatinia, M. Ramezanzadeh, G. Bahlakeh, B. Ramezanzadeh, Synthesis of a multi-functional zinc-centered nitrogen-rich graphene-like thin film from natural sources on the steel surface for achieving superior anti-corrosion properties, Corros. Sci. 178 (2021) 109077, doi:10.1016/j.corsci.2020.109077.
[54] H.H. Zhang, Y. Chen, Experimental and theoretical studies of benzaldehyde thiosemicarbazone derivatives as corrosion inhibitors for mild steel in acid media, J. Mol. Struct. 1177 (2019) 90–100, doi:10.1016/j.molstruc.2018.09.048.
[55] F. Bentiss, M. Lebrini, M. Lagrenée, Thermodynamic characterization of metal dissolution and inhibitor adsorption processes in mild steel/2,5-Bis(n-Thienyl)-1,3,4-thiadiazoles/hydrochloric acid system, Corros. Sci. 47 (12) (2005) 2915–2931, doi:10.1016/j.corsci.2005.05.034.
[56] X. Li, S. Deng, H. Fu, G. Mu, Inhibition effect of 6-benzylaminopurine on the corrosion of cold rolled steel in H2SO4 solution, Corros. Sci. 51 (3) (2009) 620–634, doi:10.1016/j.corsci.2008.12.021.
[57] T. Szauer, A. Brandt, Adsorption of oleates of various amines on iron in acidic solution, Electrochim. Acta 26 (9) (1981) 1253–1256, doi:10.1016/0013-4686(81)85107-9.
[58] H. Ashassi-Sorkhabi, B. Shaabani, D. Seifzadeh, Effect of some pyrimidinic Shciff bases on the corrosion of mild steel in hydrochloric acid solution, Electrochim. Acta 50 (16–17) (2005) 3446–3452, doi:10.1016/j.electacta.2004.12.019.
[59] K.R. Ansari, M.A. Quraishi, A. Singh, Schiff's base of pyridyl substituted triazoles as new and effective corrosion inhibitors for mild steel in hydrochloric acid solution, Corros. Sci. 79 (2014) 5–15, doi:10.1016/j.corsci.2013.10.009.
[60] N.O. Obi-Egbedi, I.B. Obot, A.O. Eseola, Synthesis, characterization and corrosion inhibition efficiency of 2-(6-methylpyridin-2-Yl)-1H-imidazo[4,5-f][1,10]phenanthroline on mild steel in sulphuric acid, Arab. J. Chem. 7 (2) (2014) 197–207, doi:10.1016/j.arabjc.2010.10.025.
[61] M. Rbaa, B. Lakhrissi, Novel oxazole and imidazole based on 8-hydroxyquinoline as a corrosion inhibition of mild steel in HCl solution: insights from experimental and computational studies, Surf. Interfaces 15 (2019) 43–59, doi:10.1016/j.surfin.2019.01.010.
[62] L. Jiang, Y. Qiang, Z. Lei, J. Wang, Z. Qin, B. Xiang, Excellent corrosion inhibition performance of novel quinoline derivatives on mild steel in HCl media: experimental and computational investigations, J. Mol. Liq. 255 (2018) 53–63, doi:10.1016/j.molliq.2018.01.133.
[63] J. Haque, K.R. Ansari, V. Srivastava, M.A. Quraishi, I.B. Obot, Pyrimidine derivatives as novel acidizing corrosion inhibitors for N80 steel useful for petroleum industry: a combined experimental and theoretical approach, J. Ind. Eng. Chem. 49 (2017) 176–188, doi:10.1016/j.jiec.2017.01.025.
[64] K.R. Ansari, M.A. Quraishi, A. Singh, S. Ramkumar, I.B. Obote, Corrosion inhibition of N80 steel in 15% HCl by pyrazolone derivatives: electrochemical, surface and quantum chemical studies, RSC Adv. 6 (29) (2016) 24130–24141, doi:10.1039/C5RA25441H.
[65] K.R. Ansari, M.A. Quraishi, Experimental and computational studies of naphthyridine derivatives as corrosion inhibitor for N80 steel in 15% hydrochloric acid, Phys. E Low-Dimens. Syst. Nanostruct. 69 (2015) 322–331, doi:10.1016/j.physe.2015.01.017.
[66] King Abdulaziz University, College of Science, Chemistry Department, Jeddah, Saudi Arabia; H. Albrakaty, R, Theoretical study of the mechanism of corrosion inhibition of carbon steel in acidic solution by 2-aminobenzothaizole and 2- mercatobenzothiazole, Int. J. Electrochem. Sci. (2018) 3535–3554, doi:10.20964/2018.04.50.
[67] M. Benabdellah, A. Aouniti, A. Dafali, B. Hammouti, M. Benkaddour, A. Yahyi, A. Ettouhami, Investigation of the inhibitive effect of triphenyltin 2-thiophene carboxylate on corrosion of steel in 2M H3PO4 solutions, Appl. Surf. Sci. 252 (23) (2006) 8341–8347, doi:10.1016/j.apsusc.2005.11.037.
[68] A. Yurt, A. Balaban, S.U. Kandemir, G. Bereket, B. Erk, Investigation on some Schiff bases as HCl corrosion inhibitors for carbon steel, Mater. Chem. Phys. 85 (2–3) (2004) 420–426, doi:10.1016/j.matchemphys.2004.01.033.
[69] Singh, A.K.; Quraishi, M.A. Piroxicam; a novel corrosion inhibitor for mild steel corrosion in HCl acid solution. 2010, 10.
[70] I. Ahamad, R. Prasad, M.A. Quraishi, Adsorption and inhibitive properties of some new mannich bases of isatin derivatives on corrosion of mild steel in acidic media, Corros. Sci. 52 (4) (2010) 1472–1481, doi:10.1016/j.corsci.2010.01.015.
[71] W. Zhang, H.-.J. Li, M. Wang, L.-.J. Wang, F. Shang, Y.-.C. Wu, Halogen-substituted acridines as highly effective corrosion inhibitors for mild steel in acid medium, J. Phys. Chem. C 122 (44) (2018) 25349–25364, doi:10.1021/acs.jpcc.8b07015.
[72] M. Scendo, The influence of adenine on corrosion of copper in chloride solutions, Corros. Sci. 50 (7) (2008) 2070–2077, doi:10.1016/j.corsci.2008.04.007.
[73] S. Martinez, I. Stern, Thermodynamic characterization of metal dissolution and inhibitor adsorption processes in the low carbon steel/mimosa tannin/sulfuric acid system, Appl. Surf. Sci. 199 (1–4) (2002) 83–89, doi:10.1016/S0169-4332(02)00546-9.
[74] Saqalli, L.; Galai, M.; Benhiba, F.; Gharda, N.; Habbadi, N.; Ghailane, R.; Ebn, M.; Peres-lucchese, Y.; Souizi, A.; Touir, R. Experimental and theoretical studies of alizarin as corrosion inhibitor for mild steel in 1.0M HCl solution. 2017, 13.

[75] L.O. Olasunkanmi, I.B. Obot, M.M. Kabanda, E.E. Ebenso, Some quinoxalin-6-Yl derivatives as corrosion inhibitors for mild steel in hydrochloric acid: experimental and theoretical studies, J. Phys. Chem. C 119 (28) (2015) 16004–16019, doi:10.1021/acs.jpcc.5b03285.
[76] P. Singh, E.E. Ebenso, L.O. Olasunkanmi, I.B. Obot, M.A. Quraishi, Electrochemical, theoretical, and surface morphological studies of corrosion inhibition effect of Green naphthyridine derivatives on mild steel in hydrochloric acid, J. Phys. Chem. C 120 (6) (2016) 3408–3419, doi:10.1021/acs.jpcc.5b11901.
[77] C.M. Fernandes, L.X. Alvarez, N.E. dos Santos, A.C. Maldonado Barrios, E.A. Ponzio, Green synthesis of 1-benzyl-4-phenyl-1h-1,2,3-triazole, its application as corrosion inhibitor for mild steel in acidic medium and new approach of classical electrochemical analyses, Corros. Sci. 149 (2019) 185–194, doi:10.1016/j.corsci.2019.01.019.
[78] X. Wang, H. Yang, F. Wang, An investigation of benzimidazole derivative as corrosion inhibitor for mild steel in different concentration HCl solutions, Corros. Sci. 53 (1) (2011) 113–121, doi:10.1016/j.corsci.2010.09.029.
[79] M. Hosseini, S.F.L. Mertens, M. Ghorbani, M.R. Arshadi, Asymmetrical Schiff bases as inhibitors of mild steel corrosion in sulphuric acid media, Mater. Chem. Phys. 78 (3) (2003) 800–808, doi:10.1016/S0254-0584(02)00390-5.
[80] C. Christodoulou, C.I. Goodier, S.A. Austin, J. Webb, G. Glass, On-site transient analysis for the corrosion assessment of reinforced concrete, Corros. Sci. 62 (2012) 176–183, doi:10.1016/j.corsci.2012.05.014.
[81] S. Ghareba, S. Omanovic, 12-Aminododecanoic acid as a corrosion inhibitor for carbon steel, Electrochim. Acta 56 (11) (2011) 3890–3898, doi:10.1016/j.electacta.2011.02.031.
[82] M. Yadav, S. Kumar, N. Kumari, I. Bahadur, E.E. Ebenso, Experimental and theoretical studies on corrosion inhibition effect of synthesized benzothiazole derivatives on mild steel in 15% HCl solution, Int. J. Electrochem. Sci. 10 (2015) 23.
[83] A. Sehmi, H.B. Ouici, A. Guendouzi, M. Ferhat, O. Benali, F. Boudjellal, Corrosion inhibition of mild steel by newly synthesized pyrazole carboxamide derivatives in HCl acid medium: experimental and theoretical studies, J. Electrochem. Soc. 167 (15) (2020) 155508, doi:10.1149/1945-7111/abab25.
[84] I. Ahamad, R. Prasad, M.A. Quraishi, Experimental and quantum chemical characterization of the adsorption of some Schiff base compounds of phthaloyl thiocarbohydrazide on the mild steel in acid solutions, Mater. Chem. Phys. 124 (2–3) (2010) 1155–1165, doi:10.1016/j.matchemphys.2010.08.051.
[85] I.B. Obot, N.O. Obi-Egbedi, A.O. Eseola, Anticorrosion potential of 2-mesityl-1H-imidazo[4,5-f][1,10]phenanthroline on mild steel in sulfuric acid solution: experimental and theoretical study, Ind. Eng. Chem. Res. 50 (4) (2011) 2098–2110, doi:10.1021/ie102034c.
[86] L.H. Madkour, S.K. Elroby, Inhibitive properties, thermodynamic, kinetics and quantum chemical calculations of polydentate schiff base compounds as corrosion inhibitors for iron in acidic and alkaline media, Int. J. Ind. Chem. 6 (3) (2015) 165–184, doi:10.1007/s40090-015-0039-7.
[87] T. Arslan, F. Kandemirli, E.E. Ebenso, I. Love, H. Alemu, Quantum chemical studies on the corrosion inhibition of some sulphonamides on mild steel in acidic medium, Corros. Sci. 51 (1) (2009) 35–47, doi:10.1016/j.corsci.2008.10.016.
[88] M.M. Kabanda, L.C. Murulana, M. Ozcan, F. Karadag, I. Dehri, I.B. Obot, E.E. Ebenso, Quantum chemical studies on the corrosion inhibition of mild steel by some triazoles and benzimidazole derivatives in acidic medium, Int. J. Electrochem. Sci. 7 (2012) 22.
[89] N. Wazzan, King Abdulaziz University, Chemistry Department, Faculty of Science, P.O Box 42805 Jeddah 21589, Saudi Arabia, Application of newly quiniline-3-carbonitriles as corrosion inhibitors on mild steel in 1.0M HCl: electrochemical measurements, HF and DFT/B3LYP calculations, Int. J. Electrochem. Sci. (2017) 9812–9828, doi:10.20964/2017.10.81.
[90] King Abdulaziz University, College of Science, Chemistry Department, Jeddah, Saudi Arabia; H. Albrakaty, R, Theoretical study of the mechanism of corrosion inhibition of carbon steel in acidic solution by 2-aminobenzothaizole and 2-mercatobenzothiazole, Int. J. Electrochem. Sci. (2018) 3535–3554, doi:10.20964/2018.04.50.
[91] R.G. Pearson, Hard and soft acids and bases—the evolution of a chemical concept, Coord. Chem. Rev. 100 (1990) 403–425, doi:10.1016/0010-8545(90)85016-L.
[92] N.O. Obi-Egbedi, I.B. Obot, M.I. El-Khaiary, S.A. Umoren, E.E. Ebenso, Computational simulation and statistical analysis on the relationship between corrosion inhibition efficiency and molecular structure of some phenanthroline derivatives on mild steel surface, Int. J. Electrochem. Sci. 6 (2011) 27.
[93] R.G. Pearson, Absolute electronegativity and hardness: application to inorganic chemistry, Inorg. Chem. 27 (4) (1988) 734–740, doi:10.1021/ic00277a030.
[94] N.A. Wazzan, I.B. Obot, S. Kaya, Theoretical modeling and molecular level insights into the corrosion inhibition activity of 2-amino-1,3,4-thiadiazole and its 5-alkyl derivatives, J. Mol. Liq. 221 (2016) 579–602, doi:10.1016/j.molliq.2016.06.011.
[95] I. Lukovits, E. Kálmán, F. Zucchi, Corrosion inhibitors—correlation between electronic structure and efficiency, Corrosion 57 (1) (2001) 3–8, doi:10.5006/1.3290328.
[96] H.T. Rahal, A.M. Abdel-Gaber, G.O. Younes, Inhibition of steel corrosion in nitric acid by sulfur containing compounds, Chem. Eng. Commun. 203 (4) (2016) 435–445, doi:10.1080/00986445.2015.1017636.
[97] R.G. Parr, L.v. Szentpály, S Liu, Electrophilicity index, J. Am. Chem. Soc. 121 (9) (1999) 1922–1924, doi:10.1021/ja983494x.
[98] N.O. Obi-Egbedi, I.B. Obot, Inhibitive properties, thermodynamic and quantum chemical studies of alloxazine on mild steel corrosion in H2SO4, Corros. Sci. 53 (1) (2011) 263–275, doi:10.1016/j.corsci.2010.09.020.
[99] E.E. Ebenso, T. Arslan, F. Kandemirlı, I. Love, C. Öğretır, M. Saracoğlu, S.A. Umoren, Theoretical studies of some sulphonamides as corrosion inhibitors for mild steel in acidic medium: theoretical studies of some sulphonamides as corrosion inhibitors, Int. J. Quantum Chem. 110 (14) (2010) 2614–2636, doi:10.1002/qua.22430.
[100] B. Gómez, N.V. Likhanova, M.A. Domínguez-Aguilar, R. Martínez-Palou, A. Vela, J.L. Gázquez, Quantum chemical study of the inhibitive properties of 2-pyridyl-azoles, J. Phys. Chem. B 110 (18) (2006) 8928–8934, doi:10.1021/jp057143y.
[101] S. Xia, M. Qiu, L. Yu, F. Liu, H. Zhao, Molecular dynamics and density functional theory study on relationship between structure of imidazoline derivatives and inhibition performance, Corros. Sci. 50 (7) (2008) 2021–2029, doi:10.1016/j.corsci.2008.04.021.
[102] J.-.L Calais, Density-Functional Theory of Atoms and Molecules, Oxford University Press, New York, Oxford, 1989 R.G. Parr and W. YangIX + 333 Pp. Price £45.00: Book Review. *Int. J. Quantum Chem.* 1993, *47* (1), 101–101, doi:10.1002/qua.560470107.
[103] K.K. Anupama, K. Ramya, A. Joseph, Electrochemical and computational aspects of surface interaction and corrosion inhibition of mild steel in hydrochloric acid by phyllanthus amarus leaf extract (PAE), J. Mol. Liq. 216 (2016) 146–155, doi:10.1016/j.molliq.2016.01.019.